TRITA-EE 2009:027
ISSN 1653-5146
ISBN 978-91-7415-317-0

SÓNIA LILÉO Auroral Electrodynamics of Plasma Boundary Regions

Auroral Electrodynamics of Plasma Boundary Regions

SÓNIA LILÉO

KTH Electrical Engineering

Doctoral Thesis in
Physical Electrotechnology
Stockholm, Sweden 2009

www.kth.se

KTH 2009

KTH Electrical Engineering

Auroral Electrodynamics of Plasma Boundary Regions

SÓNIA LILÉO

Doctoral Thesis
Space and Plasma Physics
School of Electrical Engineering
Royal Institute of Technology
Stockholm, Sweden 2009

KTH Rymd- och plasmafysik
Skolan för elektro- och systemteknik
SE-100 44 Stockholm
Sweden

TRITA-EE 2009:027
ISSN 1653-5146
ISBN 978-91-7415-317-0

Akademisk avhandling som med tillstånd av Kungl Tekniska högskolan framlägges till offentlig granskning för avläggande av teknologie doktorsexamen i fysikalisk elektroteknik fredagen den 29 maj 2009 klockan 10.00 i Sal F3, Kungl Tekniska Högskolan, Lindstedtsvägen 26, Stockholm.

© Sónia Liléo, maj 2009

Tryck: Universitetsservice US AB

Abstract

The electrodynamic coupling between the auroral ionosphere and the magnetosphere is the main subject of this thesis. Satellite measurements of electric and magnetic fields and of charged particles are used to explore three distinct plasma boundaries, magnetically linked to the nightside auroral ionosphere. These boundaries are the inner edge of the plasma sheet (PS), and the inner and the outer edges of the plasma sheet boundary layer (PSBL).

Strong ionospheric electric fields with amplitudes up to 400 mV/m may be observed in the subauroral ionosphere, in the vicinity of the ionospheric projection of the PS inner edge. Intense and dynamic auroral electric fields with local magnitudes up to 150 mV/m associated with upward ion beams and field-aligned currents are observed for the events treated here, at the inner and outer boundaries of the PSBL at an altitude of about 4-5 Earth radii, well above the acceleration region. Subauroral and auroral electric fields are the two main subjects of this thesis.

Subauroral ion drifts (SAID) are associated with poleward electric fields, occurring predominantly in the premidnight region during the substorm recovery phase. The recently revealed abnormal subauroral ion drifts (ASAID) are associated with equatorward electric fields, occurring during extended periods of low auroral activity. The results indicate that the generation mechanism of SAID can neither be regarded as a pure voltage generator nor a pure current generator, but having certain characteristics of both generator types. Ionospheric feedback appears to play a major role for the development and maintenance of the SAID electric fields. The formation of ASAID is proposed to result from the proximity and interaction between different plasma boundaries of the innermost magnetosphere during extended periods of low auroral activity.

The auroral electric fields observed in the upward current region at the PSBL inner and outer edges are associated with upward parallel electric fields, which partially decouple the high-altitude electric fields from the ionosphere. This is in contrast to the subauroral electric fields which are coupled. Multi-point measurements provided by the Cluster mission show that the observed electric fields are highly variable in space and time, revealing various types of acceleration processes. However, they appear to be tied to the boundary where they are originally formed. A case is presented where they are associated with large electromagnetic energy fluxes directed upward away from the ionosphere. The interaction between the magnetosphere and ionosphere, being more pronounced at plasma boundary regions, is important for the understanding of the formation and regulation of the highly structured auroral electric fields observed in the upward current region.

Acknowledgements

First and foremost I wish to thank my main supervisor Göran Marklund for his inspiring enthusiasm, for many fruitful discussions and for always being present as a very competent professor and as a good friend. I also, of course, thank Tomas Karlsson for his professionalism and for being such a skilled researcher and a great colleague. It has been very rewarding to work with both of you!

A special thanks to my former colleague Tommy Johansson for a good collaboration and friendship, and to Per-Arne Lindqvist for help in understanding and accessing data from the Cluster Electric Field and Wave instrument.

I especially wish to thank Ahila Thillainathan, Anita Kullen, Nickolay Ivchenko and Muhammad Shafiq for life long friendship, and Hanna Dahlgren for being such a nice office-mate, filling the room with happiness and action.

I would also like to thank the actual and former members of the administrative staff at the Space and Plasma Physics and at the Fusion groups, for their competent help and nice coffee breaks, Ingeborg Mau, Elisabeth Söderhäll, Anita Johansson, Birgitta Forsberg and Johanna Warnander. Thanks also to Lars Blomberg, Lars Bylander, Ola Carlström, Tommy Eriksson, Göran Olsson, Sverker Christenson, Torbjörn Sundberg, Soheil Sadegui and Stig Rydman for their support in many different ways.

I especially wish to thank my parents for all the valuable opportunities they have given to me and for believing in me.

Finally, I thank you Jens for all your love and precious support!

Edwin and Sofie, this thesis is dedicated to you! Here is the "Story of the beautiful lights dancing in the sky", as we use to call it!

This work was supported by the Portuguese Foundation for Science and Technology (Fundação para a Ciência e a Tecnologia) under the grant SFRH/BD/6211/2001, and by the Alfvén Laboratory Centre for Space and Fusion Plasma Physics.

List of Papers

This thesis is based on the work presented in the following papers:

1. **Figueiredo, S.**, T. Karlsson, and G. T. Marklund, Investigation of subauroral ion drifts and related field-aligned currents and ionospheric Pedersen conductivity distribution, *Ann. Geophys.*, 22, 923-934, 2004

2. **Figueiredo, S.**, G. T. Marklund, T. Karlsson, T. Johansson, Y. Ebihara, M. Ejiri, N. Ivchenko, P.-A. Lindqvist, H. Nilsson, and A. Fazakerley, Temporal and spatial evolution of discrete auroral arcs as seen by Cluster, *Ann. Geophys.*, 23, 2531-2557, 2005

3. **Liléo, S.**, G. T. Marklund, T. Karlsson, T. Johansson, P.-A. Lindqvist, A. Marchaudon, A. Fazakerley, C. Mouikis, and L. M. Kistler, Magnetosphere-ionosphere coupling during periods of extended high auroral activity: a case study, *Ann. Geophys.*, 26, 583-591, 2008

4. **Liléo, S.**, T. Karlsson, and G. T. Marklund, Statistical study on the occurrence of ASAID electric fields, *Submitted to Ann. Geophys.*, 2009

These papers are hereafter referred to as Paper 1, Paper 2, Paper 3 and Paper 4, respectively.

Publications with contributions by the author not included in the thesis:

1. Johansson, T., **S. Figueiredo**, T. Karlsson, G. Marklund, A. Fazakerley, S. Buchert, P.-A. Lindqvist, and H. Nilsson, Intense high-altitude auroral electric fields - temporal and spatial characteristics, *Ann. Geophys.*, 22, 2485-2495, 2004

2. Karlsson, T., G. T. Marklund, **S. Figueiredo**, T. Johansson, and S. Buchert, Separating spatial and temporal variations in auroral electric and magnetic fields by Cluster multipoint measurements, *Ann. Geophys.*, 22, 2463-2472, 2004

3. Marklund, G. T., T. Karlsson, **S. Figueiredo**, T. Johansson, P.-A. Lindqvist, M. André, S. Buchert, L. M. Kistler, and A. Fazakerley, Characteristics of quasi-static potential structures observed in the auroral return current region by Cluster, *Nonlinear Process. in Geophysics*, 11, 1-12, 2004

4. Johansson, T., T. Karlsson, G. Marklund, **S. Figueiredo**, P.-A. Lindqvist, and S. Buchert, A statistical study of intense electric fields at 4-7 R_E geocentric distance using Cluster, *Ann. Geophys.*, 23, 2579-2588, 2005

5. Johansson, T., G. Marklund, T. Karlsson, **S. Liléo**, P.-A. Lindqvist, A. Marchaudon, H. Nilsson, and A. Fazakerley, On the profile of intense high-altitude auroral electric fields at magnetospheric boundaries, *Ann. Geophys.*, 24, 1713-1723, 2006

6. Marklund, G., T. Johansson, **S. Liléo**, and T. Karlsson, Cluster observations of an auroral potential and associated field-aligned current reconfiguration during thinning of the plasma sheet boundary layer, *J. Geophys. Res.*, 112, doi:10.1029/2006JA011804, 2007

7. Johansson, T., G. Marklund, T. Karlsson, **S. Liléo**, P.-A. Lindqvist, H. Nilsson, and S. Buchert, Scale sizes of intense auroral electric fields observed by Cluster, *Ann. Geophys.*, 25, 2413-2425, 2007

8. Kullen, A., S. Buchert, T. Karlsson, T. Johansson, **S. Liléo**, A. Eriksson, H. Nilsson, A. Marchaudon, and A. N. Fazakerley, Plasma transport along discrete auroral arcs and its contribution to the ionospheric plasma convection, *Ann. Geophys.*, 26, 3279-3293, 2008

Contents

List of Papers vii

Contents ix

List of Figures xi

1 Introduction 1

2 The Sun-Earth Environment 3
- 2.1 The Solar Wind . . . 3
- 2.2 The Earth's Magnetic Field . . . 3
- 2.3 The Earth's Magnetosphere . . . 5
- 2.4 The Earth's Ionosphere . . . 6
- 2.5 Coupling Between the Solar Wind, the Magnetosphere, the Ionosphere and the Upper Atmosphere. . . . 7
- 2.6 Particle Drifts . . . 11
- 2.7 The Alfvén Layer . . . 14
- 2.8 Current Systems . . . 18
- 2.9 The Magnetospheric Substorm . . . 21

3 Auroral Electrodynamics 25
- 3.1 Ionospheric Currents . . . 25
- 3.2 The Auroral Current Circuit . . . 33
- 3.3 Field-Aligned Potential Structures and Coupling to the Ionosphere . 35
- 3.4 Auroral Acceleration by Alfvén Waves . . . 38
- 3.5 The Aurora . . . 40

4 Electric Fields in the Subauroral Ionosphere 43
- 4.1 Subauroral Ion Drifts . . . 43
- 4.2 Subauroral Polarization Streams . . . 46
- 4.3 Abnormal Subauroral Ion Drifts . . . 46

5 Instrumentation and Data Handling **49**
5.1 The Astrid-2 Spacecraft 49
5.2 The Cluster Spacecraft 51

6 Summary of Papers **57**
6.1 Paper 1 57
6.2 Paper 2 58
6.3 Paper 3 58
6.4 Paper 4 59

7 Discussion and Conclusions **61**

8 Future Work **65**

Bibliography **67**

List of Figures

1.1 Illustration showing the interaction of the solar wind with the Earth's magnetosphere resulting in the display of auroras. The energy transmission chain is similar to what happens in a wind power plant. Adapted from G. Marklund. 2

2.1 Sketch of the Earth's dipole magnetic field extending into a vacuum. Adapted from Wikipedia [80]. 4

2.2 Illustration of the Earth's magnetosphere and of the surrounding magnetosheath. Figure credit: European Space Agency, ESA. 5

2.3 Schematic description of a daytime midlatitude ionosphere. From P. M. Banks [6]. 7

2.4 Illustration of the magnetospheric convection driven by magnetic reconnection. The inset shows the coupled high-latitude ionospheric plasma flow forming the typical two-cell convection pattern. Adapted from Kivelson and Russell [38]. 9

2.5 Idealized two-cell convection pattern in the high-latitude ionosphere. From Baumjohann and Treumann [7]. 10

2.6 Schematic representation of the drift paths/equipotentials in the equatorial plane for cold particles, assuming an uniform magnetospheric convection electric field. From Baumjohann and Treumann [7]. 15

2.7 Schematic illustration of the drift paths on the equatorial plane for positive and negative hot plasma sheet particles. From Kivelson and Russel [38] after Vasyliunas [76]. 16

2.8 Average distribution of the magnetospheric electrons in the magnetic equatorial plane. From Kivelson and Russel [38]. 17

2.9 Schematic of the main large-scale currents that flow in the Earth's magnetosphere. From D. P. Stern [70]. 18

2.10 Typical patterns of Birkeland currents. After Iijima and Potemra [27]. . 19

2.11 Illustration of the shielding effect viewed in the magnetospheric equatorial plane with the Sun to the left. The shaded areas represent the plasma sheet, with its inner edge indicated by a heavy curve. The dashed curves are gradient-curvature drift paths. Adapted from Kivelson and Russel [38]. 20
2.12 Reconfiguration of the plasma sheet during a substorm. From Baumjohann and Treumann [7]. 22

3.1 The Cowling channel. 29
3.2 View of the auroral oval from space. Image credit: Holzworth and Meng, NSSDC, NASA 30
3.3 Conductivity structure, electric field pattern and Hall and Pedersen current circuits in the auroral region. From Baumjohann and Treumann [7]. 31
3.4 AU and AL indices for a particular substorm. From Kivelson and Russel [38]. 32
3.5 Schematic illustration of the auroral current circuit. From Marklund *et al.* [44]. 33
3.6 Schematic drawing of the equipotentials of three high-altitude electric field structures in the upward current region corresponding to (1) a total decoupling from the ionosphere, (2) a partial coupling and (3) a total coupling with the ionosphere. The electric field profiles observed when crossing above (E_a) and below (E_b) the corresponding acceleration regions are shown at the top and bottom of each panel, respectively. . . 35
3.7 A beautiful auroral display over Alaska. Image credit: H. Dahlgren. . . 40
3.8 Image of multiple discrete auroral arcs from the ASK imager located in Tromsø taken at 02:18:10 UT on 15 December 2006. Courtesy of H. Dahlgren. 41
3.9 Black auroral arc in between two discrete auroral arcs. Adapted from ESA (left picture) and T. Lövgren (right picture). 42
3.10 Image of a black auroral arc embedded in diffuse aurora from the ASK imager at 20:51:04 UT on 22 October 2006 in Tromsø. Courtesy of H. Dahlgren. 42

5.1 The Astrid-2 scientific playload. From Blomberg *et al.* [10]. 50
5.2 Cluster orbit on diagram of the Earth's magnetosphere. Image credit: ESA. 51

7.1 Schematic representation of the level of height-integrated Pedersen conductivity in the nightside ionosphere as a function of the latitude. . . . 61

Chapter 1

Introduction

The Sun is the Earth's major energy source, supporting almost all life on Earth. The most fundamental manifestations of the power delivered by the Sun are the delightful feelings of the heat and the luminosity on a sunny day. However, the Sun offers much more than heat and visible light. The advances in solar physics achieved during the last decades, partly by high-resolution ground observations, and partly by x-ray observations from satellites, have shown a highly structured and dynamic solar corona, supporting a strong and varying magnetic field. The interaction between the plasma atmosphere of the Sun and the solar magnetic field gives raise to many effects collectively called solar activity, including sunspots, solar flares, prominences, coronal mass ejections, and variations in the speed and density of the solar wind, that carries plasma and the interplanetary magnetic field through the solar system. The magnetized planets encountered by the solar wind on its way act as obstacles deflecting it. A magnetospheric cavity confining the planetary magnetic field is hence created and forms a *magnetosphere*.

The most spectacular manifestations of solar activity on Earth are the Aurora Borealis and the Aurora Australis, commonly known as Northern and Southern polar lights, respectively. Disruption of radio communications and electric power may also occur due to strong solar activity.

In a simplified view, the energy transmission chain in the Earth's magnetosphere may be compared to what takes place in a wind power plant. The wind flow drives the wind turbines that convert the wind's kinetic energy into electromagnetic energy. The converted energy is further delivered to the consumers through a power transmission network, and is finally used to power diverse electrical appliances. In a similar way, the solar wind acts as the driver carrying kinetic energy that is converted into electromagnetic energy through the interaction of the interplanetary magnetic field with the Earth's magnetic field. The resultant energy is further transmitted along the Earth's magnetic field lines into the ionosphere, powering the display of auroras. Figure 1.1 schematically illustrates this analogy. The work presented in this thesis deals primarily with the coupling between two distinct

elements of the energy transmission chain in the Sun-Earth environment, namely the ionosphere and the magnetosphere.

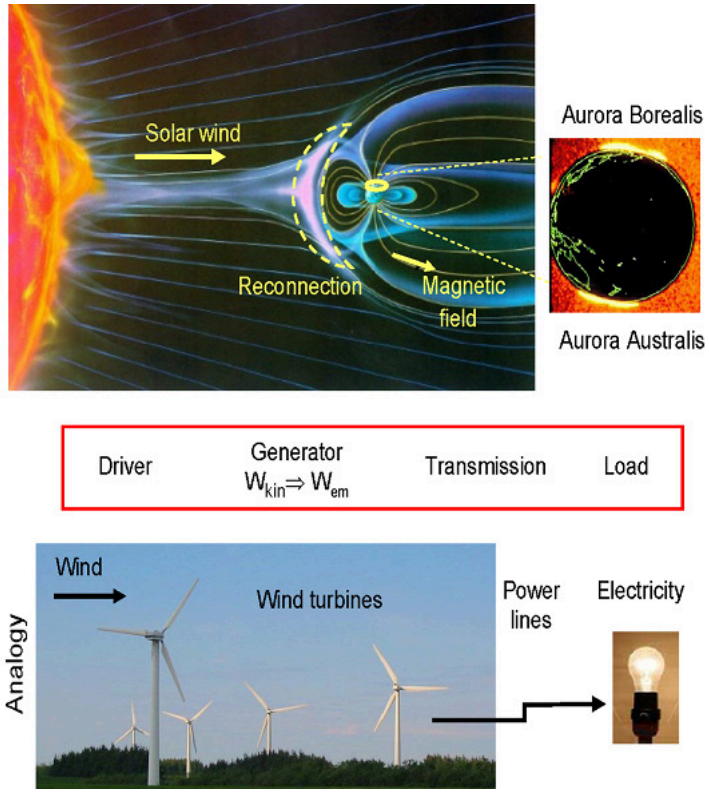

Figure 1.1: Illustration showing the interaction of the solar wind with the Earth's magnetosphere resulting in the display of auroras. The energy transmission chain is similar to what happens in a wind power plant. Adapted from G. Marklund.

This thesis is structured as follows. Chapter 2 gives a description of the fundamental properties of the Sun-Earth environment. The auroral electrodynamics is discussed in Chapter 3. Chapter 4 treats the subauroral phenomena and Chapter 5 gives an overview of the satellites Astrid-2 and Cluster, and of the instrumentation and the data handling methods used. Chapter 6 presents the summary of the main results achieved in Papers 1-4. The discussion of the results and the conclusions are presented in Chapter 7, and future work is discussed in Chapter 8. Finally, the references are given in the Bibliography, followed by the papers appended in full length.

Chapter 2

The Sun-Earth Environment

The properties of the solar wind and the configuration and plasma content of the Earth's magnetosphere determine the way the solar activity affects the Earth.

2.1 The Solar Wind

The solar wind is the flow of a highly conducting plasma composed mainly of protons and electrons (i.e., ionized hydrogen) with nearly equal densities, and a small amount of ionized helium (∼5%). The outward expansion of the solar wind results mainly from the extremely large difference in gas pressure between the solar corona and the interplanetary space. Solar magnetic field lines are frozen-in[1] to the expanding solar plasma and are therefore extended into the interplanetary medium while their footpoints remain attached in the solar atmosphere, constituting the *interplanetary magnetic field*, IMF.

Large variations in the properties of the solar wind occur as it flows from the hot and dense solar corona toward the cool and tenuous regions of the far solar system. Near the orbit of the Earth, it appears as a relatively tenuous (n_e∼7.1 cm^{-3} and n_p∼6.6 cm^{-3}) and hot[2] plasma (T_e∼12 eV and T_p∼10 eV) [25], where collisions are almost absent, flowing with a speed that typically varies between 300 and 600 km/s. The magnitude of the magnetic field frozen-in to the solar wind is about 1-10 nT close to the Earth [25].

2.2 The Earth's Magnetic Field

The magnetic field of the Earth is to a first order of approximation a dipole magnetic field with dipole axis approximately directed from the North pole to the South pole, tilted by an angle of about 11° with respect to the Earth's rotation axis (Figure 2.1).

[1] The concept of a magnetic field frozen-in to a plasma is described in Section 2.5.

[2] 1 eV (electron volt) is equivalent to 11600 K.

The field originates from currents flowing in the electrically conducting core of the Earth. It has a magnitude of $\sim$31 μT at the surface of the Earth at the magnetic equator, while at the magnetic poles the magnetic field strength is $\sim$62 μT. The equivalent *magnetic dipole moment* of the Earth, $\boldsymbol{m}$, is a vector with magnitude of $\sim 7.78 \times 10^{22}$ Am^2 and direction parallel to the dipole axis.

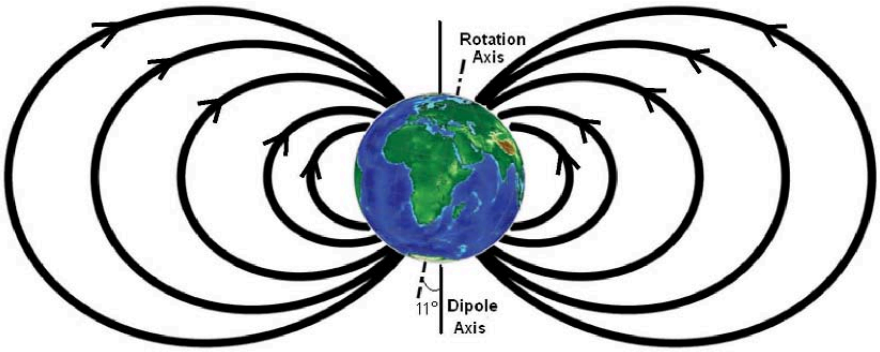

Figure 2.1: Sketch of the Earth's dipole magnetic field extending into a vacuum. Adapted from Wikipedia [80].

A highly conducting plasma surrounds the Earth and is tied to the geomagnetic field, constituting an effective obstacle to the flow of the solar wind plasma. Flowing with a velocity larger than the sound speed ($\sim$50 km/s, near the Earth), the impact of the solar wind on the Earth's magnetosphere generates a shock wave that induces a transition from supersonic flow in the upstream side, to subsonic flow downstream surrounding the Earth. The change of the flow speed is caused by irreversible processes that increase the density on the downstream side of the shock, and hence reduce the flow speed in order to conserve the mass flux. The shock wave formed in front of the Earth is called the *bow shock*, and the downstream region of subsonic flowing plasma forms the *magnetosheath*. The *magnetopause* is the boundary that separates the region dominated by the geomagnetic field, i.e. the *magnetosphere*, from the magnetosheath. Figure 2.2 is an illustration of the Earth's magnetosphere and of the surrounding magnetosheath.

The position of the magnetopause is controlled by the pressure balance between the magnetic and thermal plasma pressures of the magnetosheath and those of the magnetosphere. For a typical solar wind speed of 450 km/s, the *stand-off* location of the *nose* of the magnetopause is about 7.45 R_E (1 R_E = 1 Earth radius = $\sim$6378 km) from Earth. This location however varies dynamically with the density and the velocity of the solar wind.

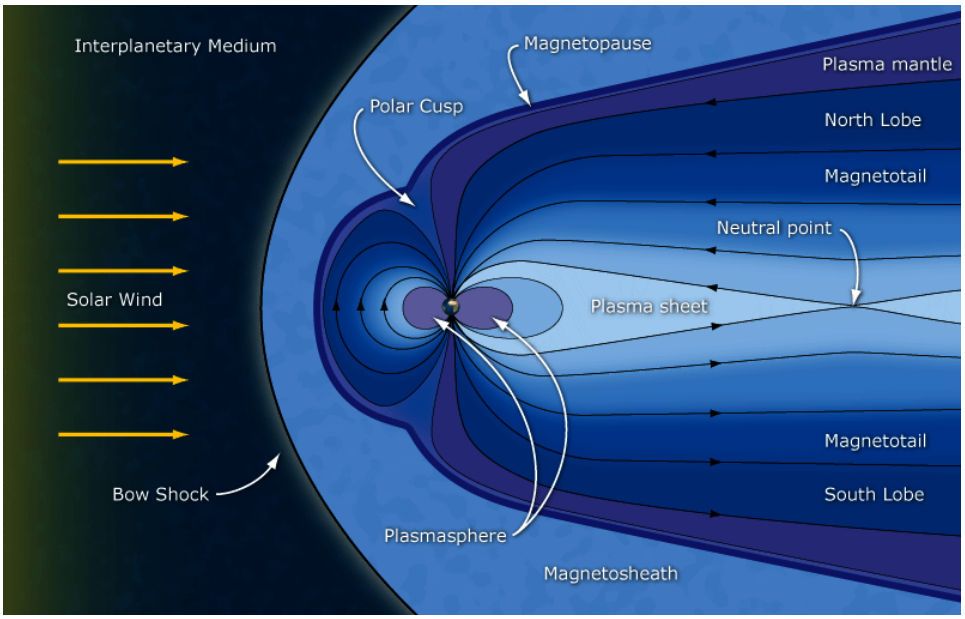

Figure 2.2: Illustration of the Earth's magnetosphere and of the surrounding magnetosheath. Figure credit: European Space Agency, ESA.

2.3 The Earth's Magnetosphere

In the magnetosphere there are a number of distinct regions defined according to the magnetic topology and to the main characteristics of the plasma populating each region (Figure 2.2). The definition of these regions may differ slightly between different authors. The definitions and characteristics described below follow those presented by Eastman et al. [15] and Wolf [83].

The nightside extended magnetic field lines form the *magnetotail*, with the magnetic field pointing away from the Earth in the south magnetotail lobe, and toward the Earth in the north magnetotail lobe. The plasma filling the magnetotail lobes is rather tenuous with a density of $\sim 10^{-2}$ cm^{-3} and a thermal energy between 10-100 eV, with very few particles in the keV range. The open magnetic field lines of the north and south magnetotail lobes map at lower altitudes to the northern and southern *polar caps* (PC), respectively

A denser (n$\sim$0.1-1 cm^{-3}) and hotter plasma (T$\sim$0.1-1 keV) fills the *plasma sheet* (PS) region in the nightside magnetosphere that is characterized by a closed magnetic field topology. The boundary between the PS (also known as *central plasma sheet*, CPS) and the magnetotail lobes is called the *plasma sheet boundary layer* (PSBL). Although spatially distinct, the width and the density of this boundary

layer can vary significantly with time ([15], Paper 2). The projection of the PS and of the PSBL to low altitudes corresponds roughly to the nighttime *auroral oval*, with the outermost edge of the PSBL mapping to the poleward edge of the auroral oval, which coincides with the PC boundary. Closer to Earth is located the *plasmasphere*, a region of cold ($T < 1eV$) and dense ($\sim 10^3 cm^{-3}$) plasma that corotates with the Earth, tied to closed magnetic field lines. The plasmasphere may be considered as an extension of the *ionosphere* (Section 2.4) and terminates with a steep density decrease at the *plasmapause*. A region of low density cold plasma exists just outside the plasmapause and is called the *plasmaspheric trough*.

In the region Earthward of the plasma sheet and overlapping with the plasmasphere are located the *radiation (or van Allen) belts* that extend to the dayside inner magnetosphere (not indicated in Figure 2.2). The radiation belts are constituted by very energetic ions and electrons with energies above ~100 keV and reaching values of hundreds of MeV, trapped between the geomagnetic mirrors. The plasma density in this region is about 1 cm^{-3}. The knowledge about this region is of great importance since the highly energetic particles of the radiation belts may induce harmful effects in instrumentation on board orbiting satellites, and are a threat to astronauts flying through this region.

Mapping to the PC dayside boundary in both hemispheres, are the *polar cusps*, characterized by a direct entry of plasma from the magnetosheath along open field lines.

2.4 The Earth's Ionosphere

The ionosphere is the transition region between the fully ionized magnetospheric plasma and the neutral atmosphere. It is located approximately between 50 and 1000 km altitude [6]. The solar ultraviolet (UV) radiation and the precipitation of energetic particles coming from the galaxy (cosmic rays), from the Sun and from the magnetosphere, are the main ionization sources of the ionosphere. Photoionization (ionization by solar UV radiation) depends on latitude, time of the day and on season, dominating in the dayside ionosphere. Impact ionization (ionization by energetic precipitating particles) dominates mainly in the nightside ionosphere at high magnetic latitudes.

The altitudinal variation of the density of the different atmospheric constituents combined with the different penetration depths of the components of the incident solar radiation spectrum, result in a structured altitude distribution of ionospheric density, with several distinct maxima located at different altitudes, named the ionospheric D, E and F layers. Figure 2.3 is a schematic picture of the altitude electron density for the daytime midlatitude ionosphere, showing the different layers with the respective dominant ion constituents and the corresponding dominant ionization sources.

In the nighttime ionosphere the altitude distribution of the ionospheric density is less structured showing two main layers: the E layer corresponding to a peak of

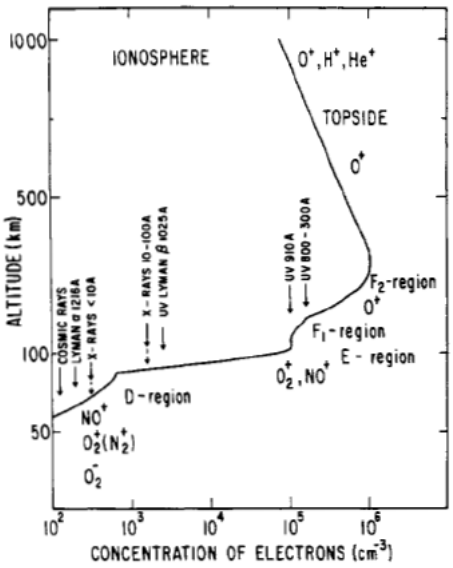

Figure 2.3: Schematic description of a daytime midlatitude ionosphere. From P. M. Banks [6].

the electron density of $\sim 2\times10^3$ cm^{-3} located at an altitude of $\sim$100 km, and the F layer with a peak in the electron density of $\sim$2-4$\times10^5$ cm^{-3} located at an altitude of 300-350 km altitude [23].

2.5 Coupling Between the Solar Wind, the Magnetosphere, the Ionosphere and the Upper Atmosphere.

One of the primary objectives of space plasma physics is the understanding of the coupling mechanisms between the solar wind, the magnetosphere, the ionosphere and the atmosphere. These coupling mechanisms are of major importance for the transmission of power from the impinging solar wind to the magnetosphere and the ionosphere where it is dissipated.

Magnetic Reconnection

The coupling between the solar wind and the magnetosphere is thought to be mainly realized by magnetic reconnection occurring in the dayside magnetopause and in the far magnetotail.

The concept of magnetic field lines frozen-in to plasmas is a main topic within ideal magnetohydrodynamics (MHD) that treats electrically conducting fluids that have low resistivity, i.e. perfectly conducting fluids. In ideal MHD the magnetic field lines are tied to the fluid as long as its resistivity is negligible. Reconnection between different magnetic field lines is under these conditions not possible, and the field is said to be *frozen-in* to the plasma.

The frozen-in criterion may however break down in thin boundaries separating different plasma domains, where magnetic diffusion becomes dominant over convection. An example of such a boundary is the magnetopause separating the IMF frozen-in to the solar wind plasma from the geomagnetic field frozen-in to the magnetospheric plasma. When ideal MHD breaks down locally at the dayside magnetopause, and if the IMF is southward oriented, merging between the oppositely directed IMF lines and the geomagnetic field lines may occur, allowing the transport of mass, momentum and energy across the magnetopause. A similar magnetic reconnection process may also occur in the neutral current sheet that separates the oppositely directed magnetic field lines of the northern and southern lobes in the far magnetotail. Energy that has been stored in the magnetotail field may then be released into the magnetosphere as a result of the reconnection of the magnetotail field lines. This topic is further described in Section 2.9.

The Convection Electric Field

As a consequence of the reconnection between the IMF and the geomagnetic field at the dayside magnetopause, a large scale magnetospheric convection electric field is created. It is induced when the reconnected open field lines sweep over the polar caps toward the tail. This motion is schematically illustrated in Figure 2.4.

After reconnection of the IMF line 1' with the geomagnetic field line 1, the resulting open field line 2 sweeps over the polar cap toward the distant tail (field line 5). The electric field induced in the frozen-in plasma when swept antisunward (at the velocity $\mathbf{v}$) is dawn-to-dusk oriented ($\mathbf{E} = -\mathbf{v} \times \mathbf{B}$) and maps along the magnetic field lines (considered to be equipotentials) down to the polar cap region. An antisunward $\mathbf{E} \times \mathbf{B}$ drift (Section 2.6) of the ionospheric plasma is consequently generated in the polar cap region. This plasma motion is illustrated in the inset of Figure 2.4 by the antisunward plasma flow lines drawn over the polar cap. The typical potential difference between the dawn and dusk magnetopause is about 50-100 kV [7], which corresponds to a magnetospheric convection electric field with magnitude between 0.2 and 0.5 mV/m, assuming a cross-section of the magnetosphere of about $30R_E$. The ionospheric convection electric field has typical values of 20-50 mV/m in the auroral zone.

When the magnetic field lines of the northern and southern lobes are stretched into the magnetotail (field lines 5 and 5' of Figure 2.4), they may merge together turning the magnetic field more dipole like. The magnetic force associated with the dipolarization of the magnetic field acts together with the drift due to the magnetospheric convection electric field resulting in a sunward motion of plasma

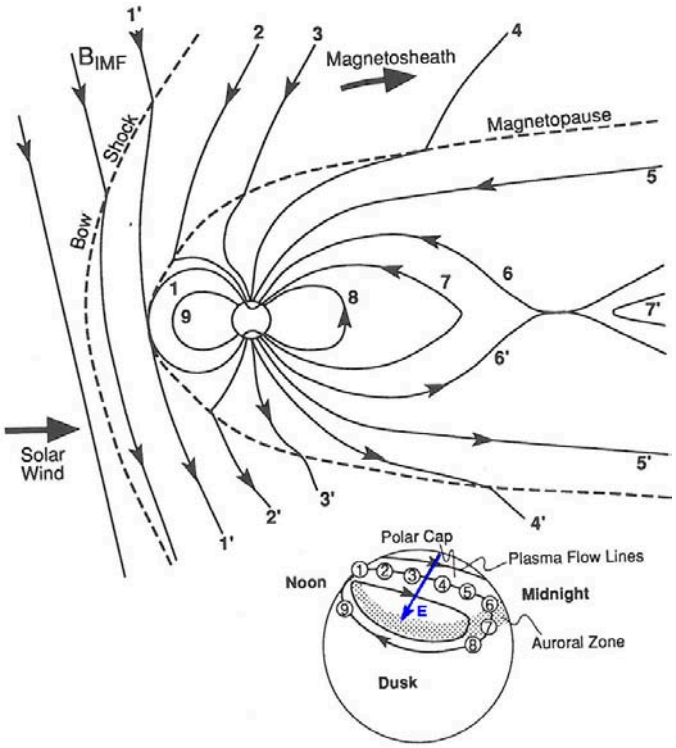

Figure 2.4: Illustration of the magnetospheric convection driven by magnetic reconnection. The inset shows the coupled high-latitude ionospheric plasma flow forming the typical two-cell convection pattern. Adapted from Kivelson and Russell [38].

on closed field lines toward the Earth and around the flanks of the magnetosphere (field lines 8 and 9). The electric field induced in the plasma moving with these closed field lines around the flanks maps down along the magnetic field lines to the auroral zone as a dusk-dawn oriented electric field that generates a return sunward flow of the ionospheric plasma in this region. This creates the two-cell ionospheric convection pattern illustrated in Figure 2.5, typically observed during periods of southward IMF. For northward IMF, the ionospheric convection is more structured and is confined to higher latitudes. The ionospheric convection pattern becomes more complex and may have three or four cells.

As illustrated in Figure 2.5, the convection electric field points duskward in the polar cap, poleward in the evening sector and equatorward in the morning sector, and the ionospheric plasma drifts along the corresponding equipotentials, in the direction shown in the inset of Figure 2.4.

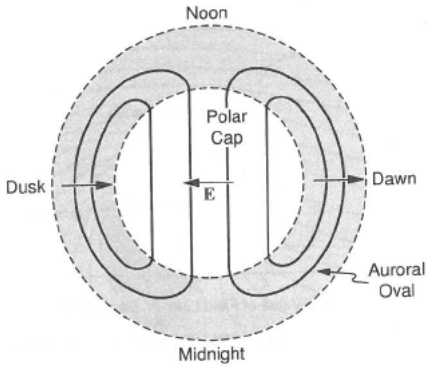

Figure 2.5: Idealized two-cell convection pattern in the high-latitude ionosphere. From Baumjohann and Treumann [7].

The ionospheric plasma convection generated by the mapping of the magnetospheric convection electric field is one example of the magnetosphere-ionosphere coupling. The mapping of electric fields along the geomagnetic field lines relies on the assumption that the electric potential is constant along the magnetic field lines. This is in general true in the ionosphere since the conductivity parallel to the magnetic field is substantially larger than that perpendicular to the field. However, the existence of high-altitude electric fields directed along magnetic field lines with footpoints in the auroral oval is well known ([50, 44] and Paper 3). This topic is discussed in more detail in Section 3.2.

The convection electric field generated from the interaction of the solar wind with the geomagnetic field is a major driver of the bulk drift motion of plasma in the magnetosphere. Another major contribution arises from the corotation electric field associated with the rotation of the Earth.

The Corotation Electric Field

The neutral atmosphere surrounding the Earth is dragged via viscous interaction with the corotating solid body of the Earth. Due to collisions between the neutral atmospheric particles and the ions and electrons constituting the ionospheric plasma, the lower parts of the ionosphere are forced into corotation as well. Since the magnetic field lines are equipotentials this corotation can be communicated also to the higher altitudes corresponding to the plasmapshere. For a non-corotating observer, the corotation of the ionospheric plasma through the magnetic environment of the Earth is equivalent to an electric field

$$\mathbf{E} = -\mathbf{v} \times \mathbf{B} = -(\Omega_E \times \mathbf{r}) \times \mathbf{B} \tag{2.1}$$

where Ω_E is the Earth's angular velocity vector pointing vertically from the South to the North Pole, and $\mathbf{r}$ is the position vector from the center of the Earth. The resultant corotation electric field is directed radially inward (toward magnetic shells with lower L-values). The magnitude of the corotational electric field in the equatorial plasmapause (typical geocentric distance of $4.5R_E$) is $\sim 0.7mV/m$ and falls off with the square of the geocentric distance for a dipole magnetic field.

2.6 Particle Drifts

The single particle motion approach for the description of a plasma is valid for low density plasmas where collective effects are negligible and when the motion of the charged particles does not affect the external magnetic field. In this approach, the motion of charged particles in a magnetic field is characterized by the gyration around a guiding center in the plane perpendicular to the magnetic field, and by the parallel motion of the guiding center along the magnetic field lines. When an electric field is also applied or in cases of a non-uniform magnetic field, other terms are added to the drift motion of the guiding center deviating it from the field-aligned direction.

The gyration of a charged particle in the plane perpendicular to a magnetic field $\mathbf{B}$, is ruled by the Lorentz force. The equation of motion is therefore

$$m\frac{d\mathbf{v}}{dt} = q\mathbf{v} \times \mathbf{B} \tag{2.2}$$

where m and q and $\mathbf{v}$ are the particle's mass, charge and velocity vector, respectively. Multiplying Equation 2.2 with the particle's velocity $\mathbf{v}$, results in

$$\mathbf{v} \cdot m\frac{d\mathbf{v}}{dt} = \mathbf{v} \cdot (q\mathbf{v} \times \mathbf{B}) \tag{2.3}$$

$$\frac{d}{dt}\left(\frac{1}{2}mv^2\right) = 0 \tag{2.4}$$

which implies that the total kinetic energy of the particle, $W = \frac{1}{2}mv^2$, is a constant of the motion. Since the Lorentz force is perpendicular to the magnetic field, and in absence of other external forces, there is no force accelerating the particle in the field-aligned direction. The field-aligned component of the particle's velocity, $v_{||}$, is therefore constant, as well as the parallel component of the kinetic energy, $W_{||}$. Since W and $W_{||}$ are both constants of the motion, it results that the perpendicular component of the kinetic energy, $W_\perp$, and hence the magnitude of the perpendicular component of the velocity, $v_\perp$, are also constants. Hence, the particle describes a circular motion with constant speed around a guiding center that has an uniform motion along the magnetic field. The radius of the circular motion, r_L, follows from the perpendicular component of the equation of motion (2.2) together with the definition of centripetal acceleration, $a = \frac{v_\perp^2}{r_L}$.

$$m\frac{dv_\perp}{dt} = qv_\perp B \tag{2.5}$$

$$r_L = \frac{mv_\perp}{qB} \tag{2.6}$$

r_L is called the *Larmor radius* or *cyclotron radius*. This definition is equivalent to

$$r_L = \frac{144}{B}\sqrt{W_\perp} \tag{2.7}$$

for protons, and

$$r_L = \frac{3.37}{B}\sqrt{W_\perp} \tag{2.8}$$

for electrons, with $W_\perp$ given in electron volts, B in nanoteslas and r_L in kilometers.

Using Equation 2.6, the cyclotron frequency, $\omega_c = \frac{v_\perp}{r_L}$, is given by

$$\omega_c = \frac{qB}{m}. \tag{2.9}$$

A particle with charge q and an uniform circular motion with speed $v_\perp$, generates a current loop with magnetic moment $\mathbf{m} = IA\hat{\mathbf{n}}$, where $I = \frac{|q|}{T_c}$ is the average current intensity, T_c is the period of the circular motion, $A = \pi r_L^2$ is the area of the loop and $\hat{\mathbf{n}}$ is an unity vector perpendicular to the loop's surface pointing according to the right-hand rule applied to the flow direction of the current (same/opposite as the direction of a gyrating positive/negative charge). In space plasma physics the absolute value of $\mathbf{m}$ is generally designated by μ. Using equations 2.6 and 2.9 results

$$\mu = \frac{W_\perp}{B}, \tag{2.10}$$

which is constant for a static and uniform magnetic field.

Since positively charged particles gyrate in the left-hand sense in the plane perpendicular to the applied magnetic field, while negatively charged particles gyrate in the right-hand sense, the current flows in the left-hand sense for both positive and negative charges. The magnetic moment is therefore directed opposite to the magnetic field. Consequently a magnetized plasma is said to be *diamagnetic*. In the presence of a large amount of particles the magnetic field induced by the motion of the charged particles may reduce significantly the magnitude of the externally applied magnetic field.

It may be shown that for slowly varying magnetic fields (time scales larger than the gyroperiod), the magnetic moment is conserved. It is therefore an *adiabatic invariant*. The conservation of μ and of energy has an important consequence for the motion of charged particles in the non-uniform geomagnetic field. It implies that a charged particle gyrating in turn of a guiding center moving along a geomagnetic field line becomes trapped between the geomagnetic mirrors, describing a bounce

motion between the hemispheres. Only the particles filling the loss cone of the geomagnetic mirror will achieve the upper atmosphere and produce aurora. These are particles moving very close to or parallel to the field line, whose velocity vector makes an angle with the geomagnetic field direction at the magnetic equator (i.e. *pitch-angle*) less than the *loss cone angle*, θ_m . Using conservation of the magnetic moment and of energy during the bounce motion of a particle along a geomagnetic field line, follows that the loss cone angle θ_m is defined as

$$\theta_m = arcsin\sqrt{\frac{B_0}{B_t}} \tag{2.11}$$

where B_0 is the magnitude of the magnetic field at the equatorial footpoint of a magnetic field line (weak-field region), and B_t is the magnitude at the turning point (strong-field region) of the motion of a particle along the same field line.

$\mathbf{E} \times \mathbf{B}$ Drift

Geophysical plasmas are generally under the influence of both magnetic and electric fields. Considering the case of spatially uniform and static electric and magnetic fields, a charged particle will drift with a velocity

$$\mathbf{v} = \frac{\mathbf{E} \times \mathbf{B}}{B^2} \tag{2.12}$$

in the direction perpendicular to both electric and magnetic fields. The $\mathbf{E} \times \mathbf{B}$ drift velocity is independent of charge, mass and energy, implying that all particles drift in the same direction and at the same velocity. The $\mathbf{E} \times \mathbf{B}$ drift produces therefore no net current density, once all particles drift at the same velocity and since a plasma is assumed to be electrically neutral. The $\mathbf{E} \times \mathbf{B}$ motion also does not change the total energy of a particle, since the particles drift in the direction perpendicular to the electric field, i.e. along equipotential contours.

An example of $\mathbf{E} \times \mathbf{B}$ plasma drift is the sunward motion of particles on closed field lines in the plasma sheet due to the magnetospheric convection electric field.

In the vicinity of plasma boundaries and small scale structures in a plasma, when the electric field may change considerably over one Larmor radius, an additional term must be added to the $\mathbf{E} \times \mathbf{B}$ drift velocity. Equation 2.12 is in this case replaced by

$$\mathbf{v} = \left(1 + \frac{1}{4} r_L^2 \nabla^2\right) \frac{\mathbf{E} \times \mathbf{B}}{B^2}. \tag{2.13}$$

Equation 2.13 takes into account the spatial variation of the electric field. This is called the *finite Larmor radius effect.*

Magnetic Gradient and Curvature Drifts

The geomagnetic field is far from being spatially uniform. The gradient of the magnetic field intensity in the radial direction together with the centrifugal force due to the curvature of the field lines, lead to a drift motion of charged particles in the direction perpendicular to both the magnetic field and the radial direction.

The gradient drift motion is given by the following expression,

$$\mathbf{v}_G = \frac{1}{2} v_\perp^2 \frac{m}{q} \frac{\mathbf{B} \times \nabla B}{B^3}. \tag{2.14}$$

The curvature drift velocity is equal to

$$\mathbf{v}_C = v_{||}^2 \frac{m}{q} \frac{\mathbf{R}_C \times \mathbf{B}}{R_C^2 B^2} = v_{||}^2 \frac{m}{q} \frac{\mathbf{B} \times \nabla B}{B^3}, \tag{2.15}$$

where $\mathbf{R}_C$ is a vector with magnitude equal to the radius of curvature of the field line, pointing radially outward from the center of the Earth. In vaccum one have $\nabla \times \mathbf{B} = 0$. In cylindrical coordinates results that $\frac{\nabla B}{B} = -\frac{\mathbf{R}_C}{R_C^2}$, justifying the equivalence in Equation 2.15. The total drift velocity due to the gradient and the curvature of the magnetic field is therefore given by

$$\mathbf{v}_G + \mathbf{v}_C = (v_{||}^2 + \frac{1}{2} v_\perp^2) \frac{m}{q} \frac{\mathbf{B} \times \nabla B}{B^3}. \tag{2.16}$$

This drift velocity is dependent on the particle's charge meaning that positively and negatively charged particles drift in opposite directions giving rise to currents. Noting the dependence on the particles' energy, one may conclude that it is the motion of the high-energetic particles, *hot particles*, that is more influenced by the gradient and curvature drifts. This drift motion does not necessarily occur along equipotential contours implying that the particles may gain or lose energy as they drift into lower or higher electrostatic potential contours, respectively.

The energetic charged particles forming the radiation belts (mentioned in Section 2.3) are particles that are trapped between the geomagnetic mirrors, gyrating around a guiding center that describes a bounce motion between the hemispheres. Moreover, the motion of these energetic particles is strongly affected by the gradient and curvature drifts, resulting in a circular motion around the Earth with positively charged particles drifting westward and electrons drifting eastward. These drift motions produce a current with intensity proportional to the kinetic energy of the drifting particles, and that encircles the Earth in the westward direction. This current is called the *ring current* and is the topic of further discussion in Section 2.8.

2.7 The Alfvén Layer

The dawn-dusk directed magnetospheric convection electric field causes the nightside plasma sheet plasma to $\mathbf{E}\times\mathbf{B}$ drift towards the Earth and around the dusk

and dawn flanks towards the Sun, as described in Section 2.5. When close enough to the Earth, the drift motion of the particles will also be affected by the gradient and curvature of the geomagnetic field, and by the corotational motion of the Earth. Considering the simple case of cold particles (these will not be affected by the gradient-curvature drift), their drift paths in the equatorial plane may be schematically represented as shown in Figure 2.6.

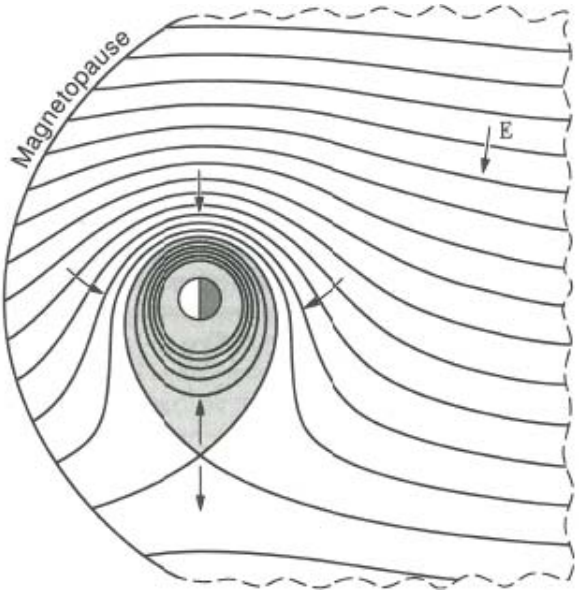

Figure 2.6: Schematic representation of the drift paths/equipotentials in the equatorial plane for cold particles, assuming an uniform magnetospheric convection electric field. From Baumjohann and Treumann [7].

Near the Earth the corotational electric field dominates over the convection electric field causing the particles to drift in closed paths around the Earth, moving eastward. The region where the corotation dominates over convectiom is the plasmasphere (gray shaded region in Figure 2.6). Outside the plasmasphere, the drift motion of the particles is controlled by the dawn-dusk convection electric field. Hence, the particles drift sunward on open drift paths. On the dawn flank of the magnetosphere, both the convection and the corotational electric fields make the plasma drift eastward. However, on the dusk flank, the convection electric field makes the plasma drift westward (sunward) while the corotational electric field drives the plasma in the eastward direction. The point where the convection electric field totally balances the oppositely directed corotational electric field is called the *stagnation point*. Here the flow velocity is zero. The drift path separating the

cold plasma of the plasmasphere drifting continuously around the Earth on closed trajectories, from the cold plasma drifting on open trajectories from the tail to the dayside magnetopause, is called the *separatrix*.

Due to the deceleration of the plasmaspheric particles when approaching the stagnation point, their flow lines have to spread out. A bulge is therefore formed in the dusk region of the plasmasphere. The radial location of the stagnation point is determined by the magnitude of the magnetospheric convection electric field. An increase of the magnitude of the convection electric field will reduce the distance of the stagnation point, and the size of the plasmasphere. The plasmapause therefore moves closer to the Earth. Another aspect resulting from an enhancement of the convection electric field is the movement of the bulge toward local noon and the erosion of the outer plasmasphere. These result from the different delay-times of the separatrix and the plasmapause to an increase of the convection electric field. While the separatrix moves instantaneously closer to the Earth, the plasmapause takes longer time. Consequently, the particles of the outer plasmasphere that were primarily moving in closed paths become moving along open trajectories and are lost to the dayside magnetosphere.

Let us now consider what happens with the hot particles of the plasma sheet when $\mathbf{E}\times\mathbf{B}$ drifting Earthward under the influence of the convection electric field. Besides experiencing the influence of the Earth's corotational electric field, these particles are also subject to the gradient-curvature drift. Since positively and negatively charged particles gradient-curvature drift in opposite directions, the configuration of the drift trajectories will be different for the positive ions and for the electrons of the plasma sheet. The plasma sheet positive ions are able to penetrate deeper into the inner magnetosphere on the dusk side, while the electrons penetrate closer to Earth on the dawn side, as schematically illustrated in Figure 2.7.

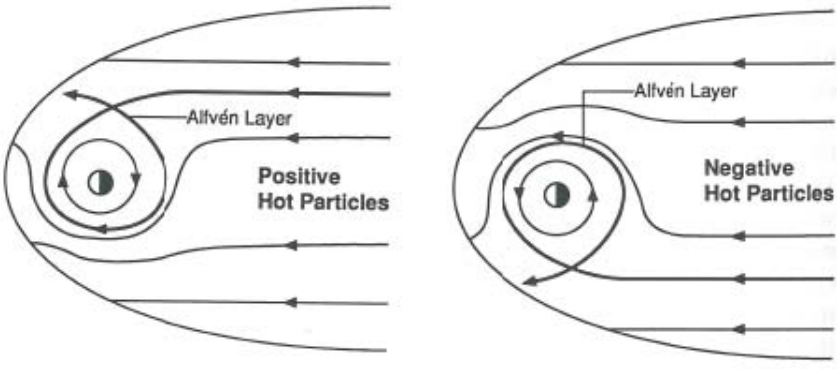

Figure 2.7: Schematic illustration of the drift paths on the equatorial plane for positive and negative hot plasma sheet particles. From Kivelson and Russel [38] after Vasyliunas [76].

The heavy lines represented in the left and right sides of Figure 2.7 indicate the innermost position of the open trajectories of the plasma sheet ions and electrons, respectively, in the equatorial plane. These separatrixis are called *Alfvén layers* and represent the inner edges of the ion and the electron plasma sheets in the equatorial plane, respectively. The radial distance of the stagnation point is proportional to the energy of the particles (more energetic particles have larger drift velocities and consequently a larger bulge is formed). This explains the typical configuration of the inner magnetosphere, with the inner edge of the electron plasma sheet being located farther from Earth than the plasmapause, as shown in Figure 2.8.

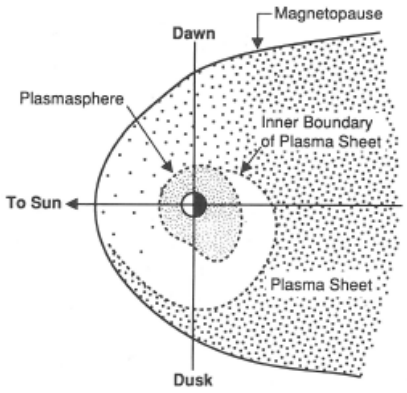

Figure 2.8: Average distribution of the magnetospheric electrons in the magnetic equatorial plane. From Kivelson and Russel [38].

Since the plasma sheet electrons are hotter than the plasmaspheric electrons, the plasmapause is located Earthward of the inner edge of the electron plasma sheet. Moreover, the inner edge of the electron plasma sheet lies closer to Earth on the dawnside than on the duskside. Cold magnetospheric plasma drifting sunward on open paths fill the region between the plasmapause and the plasma sheet inner edge. This region is the cold plasmaspheric trough located just outside the plasmapause. The location of the inner edge of the plasma sheet also depends on the magnitude of the convection electric field, as does the location of the plasmapause. An inward motion of both the plasmapause and the inner edge of the plasma sheet is normally observed during periods of enhanced convection. This explains the expansion (contraction) of the auroral oval toward lower (higher) latitudes that typically occurs during periods of large (weak) magnetic activity.

The dynamics of the locations of the ion and electron plasma sheet inner edges relative to each other and to the location of the plasmapause are of importance for the formation of subauroral electric fields. These are subject of investigation in Papers 1 and 4, and are further described in Chapter 4.

2.8 Current Systems

There are several large-scale current systems flowing in the Earth's magnetosphere. Some of these currents arise as the result of the motion of plasma under the influence of the geomagnetic field; others are consequences of the magnetospheric field structure, or generated as a response to an applied voltage. Magnetospheric currents may also be regarded as the source of magnetic fields that distort the Earth's magnetic field. Figure 2.9 shows a schematic representation of the main magnetospheric current systems described in this section.

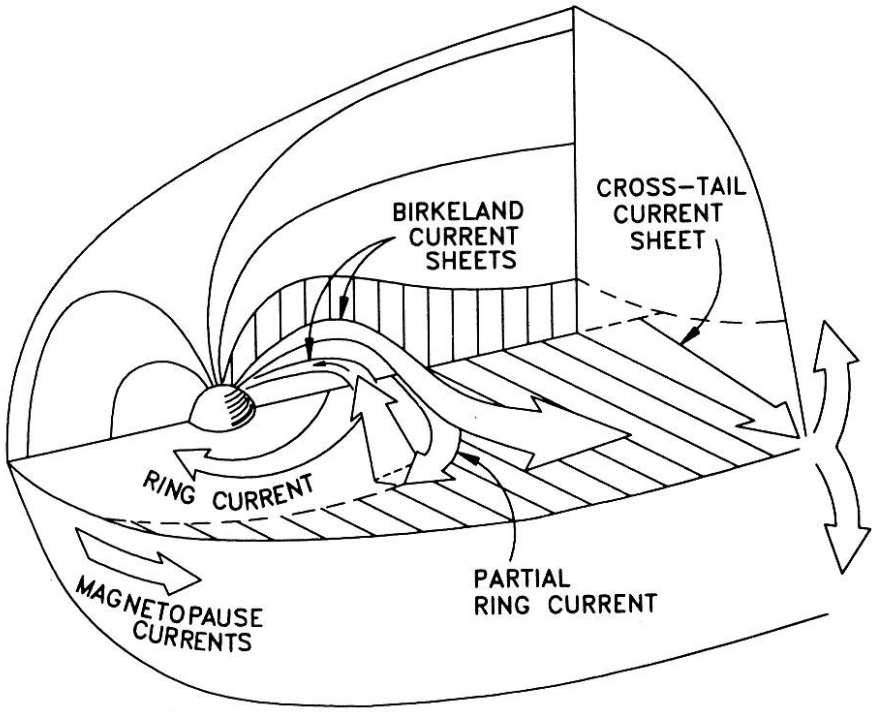

Figure 2.9: Schematic of the main large-scale currents that flow in the Earth's magnetosphere. From D. P. Stern [70].

Separating the oppositely directed magnetic field lines of the northern and the southern magnetotail lobes is the cross-tail current sheet, also called neutral current sheet. The density of the current flowing in the neutral current sheet may be estimated by using Ampère's law. A current density of 0.2 MA per each R_E of the length of the tail results assuming a tail magnetic field of 20 nT. The cross-tail current flows from dawn to dusk where it bifurcates at the magnetopause into

the *magnetopause currents*, flowing northward and southward around the magnetopause and closing on the dawn flank. At the near-equatorial dayside magnetopause, currents flow along the boundary from dawn to dusk, as illustrated in Figure 2.9. The dayside magnetopause currents create a magnetic field that cancels the dipole field outside the magnetopause and intensifies the dipole field just inside the magnetopause. They also contribute with a $\mathbf{j}\times\mathbf{B}$ force that deflects the solar wind plasma. In the simplest case where there is no coupling between the solar wind and the geomagnetic field, the magnetopause currents close with themselves and with the neutral current flowing in the tail, forming a current sheet that confines the geomagnetic field.

The ring current is generated from the combination of the gradient and curvature drifts of the energetic particles trapped in the radiation belts, resulting in a circular drift around the Earth that is in opposite direction for ions, moving westward, and electrons moving eastward (as mentioned in Section 2.6). A current flowing westward is therefore generated, carried mainly by ions in the medium-energy range from ~10 keV to a few hundreds of keV. The electrons trapped in the radiation belts are considerably cooler than the trapped ions, and have therefore a relatively minor contribution to the total gradient-curvature drift current. During periods of low magnetic activity, the bulk position of the ring current is located at a geocentric distance of about 6 R_E [30], with a average current density of $\sim$ 1 to 4 nAm^{-2}, and is mainly composed by protons originated from the solar wind plasma. During periods of high magnetic activity the bulk position of the ring current is located at about 5 R_E and the current density may exceed values of ~7 nAm^{-2}. Ions of ionospheric origin (O^+ and protons) are the main constituents of the ring current during intense magnetic activity.

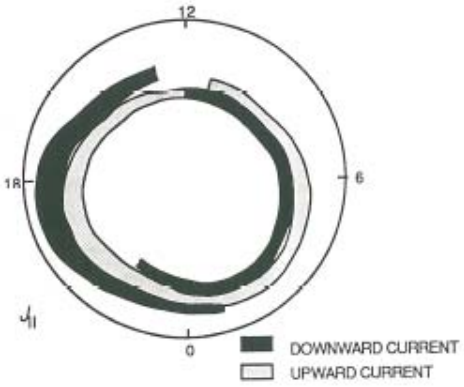

Figure 2.10: Typical patterns of Birkeland currents. After Iijima and Potemra [27].

Figure 2.10 illustrates the system of Birkeland currents (also shown in Figure 2.9) linking the magnetosphere with the auroral ionosphere. Dark shaded regions

correspond to downward field-aligned currents (FAC) flowing into the ionosphere, and light shaded regions to upward FAC flowing away from the ionosphere [27]. The system of FAC flowing at higher latitudes into the ionosphere in the dawn sector and away from the ionosphere in the dusk sector is called the *region-1 Birkeland currents*. This region is expected to connect to the outer boundary of the plasma sheet. The *region-2 Birkeland currents* are located at lower latitudes and flow into the ionosphere in the dusk sector and away from the ionosphere in the dawn sector connecting to the partial ring current (Figure 2.9) that flows in the equatorial inner magnetosphere. Pressure gradients near the inner edge of the plasma sheet are the main cause for the formation of the region-2 Birkeland currents, and may significantly influence the overall convection pattern [77, 82].

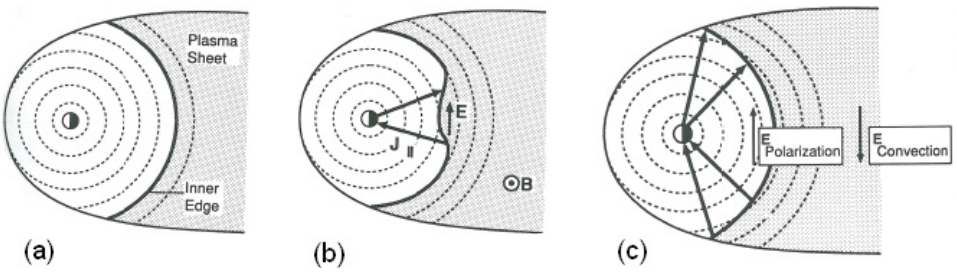

Figure 2.11: Illustration of the shielding effect viewed in the magnetospheric equatorial plane with the Sun to the left. The shaded areas represent the plasma sheet, with its inner edge indicated by a heavy curve. The dashed curves are gradient-curvature drift paths. Adapted from Kivelson and Russel [38].

Figure 2.11 illustrates schematically what happens when a bump is formed in the plasma sheet inner edge (panel (b)) disturbing the equilibrium configuration in which the inner edge is parallel to the contours of gradient-curvature drift (panel (a)). The formation of a bump in the plasma sheet inner edge requires an extra gradient-curvature drift current flowing through the bump in the westward direction. The closure of this partial ring current is done through field-aligned currents flowing into the ionosphere in the west side of the bump and up from the ionosphere in the east side. This system of field-aligned currents polarizes the ionosphere positively at the ionospheric end of the downward FAC in the west side and negatively in the east ionospheric end, with an eastward perpendicular current flowing through the ionosphere and closing the system. Assuming that the magnetic field lines are equipotential lines, the west side of the bump will be at a higher potential than the east side, generating a polarization electric field directed eastward that leads to the motion of the plasma sheet inner edge back into line.

Panel (c) of Figure 2.11 shows the effect of the dawn-dusk convection electric field imposed across the tail. The induced sunward drift motion of the plasma sheet particles will result in a deformation of the plasma sheet inner edge with the night

side plasma sheet moving closer to Earth and the morning and evening sides moving further away. As described in the simplest case a localized bump (panel (b)), this deformation of the plasma sheet inner edge requires the flow of a westward partial ring current flowing in the nightside region which is connected to the ionosphere by downward field-aligned currents in the dusk and premidnight sector and by upward field-aligned currents in the postmidnight and dawn sector. These field-aligned currents constitute the region-2 Birkeland current system. In order to enable current closure of the region-2 current system, a dusk-dawn polarization electric field is formed in the ionosphere that maps to the magnetosphere and opposes the magnetospheric convection electric field. In steady-state conditions the polarization electric field balances the applied convection electric field and cancels the original sunward motion of the plasma sheet inner edge. The inner edge of the plasma sheet tends therefore to shield the inner magnetosphere and the mid- and lowlatitude ionosphere from the convection electric field, which is called the *shielding effect*.

The shielding effect depends on the pressure in the inner magnetosphere [81] and on the ionospheric conductivity [68], and is sometimes quite ineffective (*under-shielding*) due to time variations in the applied convection potential. *Overshielding* may also occur, when the shielding electric field becomes larger than the convection electric field. This occurs for example when the IMF suddenly turns northward after a prolonged southward orientation. Associated with the sudden IMF northward turning, a rapid decrease of the convection electric field occurs, while the magnitude of the pressure gradients in the inner magnetosphere take longer time to respond, remaining therefore strong for a while and contributing for an intense shielding electric field [34, 69].

The effectiveness of the shielding mechanism preventing the penetration of the convection electric field into the midlatitude region is of major importance for the formation of electric fields in the subauroral region (Chapter 4, Paper 1 and Paper 4).

2.9 The Magnetospheric Substorm

The coupling between the solar wind and the magnetosphere was mentioned in Section 2.5. Merging of the IMF carried by the solar wind plasma with the geomagnetic field at the frontside magnetopause enables the transport of energy and plasma from the solar wind into the magnetosphere. The rate of energy input is dependent on the solar wind velocity and on the magnitude and the direction of the IMF. When the IMF turns southward, the merging of IMF and geomagnetic field is highly enhanced and leads to a sequence of events in the magnetosphere and ionosphere referred to as *magnetospheric substorm*. The different phases of a magnetospheric substorm are detailed below. Note that substorms however is still a matter of active debate, with different interpretations being presented by different authors. The description below follows the ideas presented by Baumjohann and

Treumann [7].

Growth Phase

Following the enhancement of the dayside reconnection rate associated with a southward turning of the IMF, the merged magnetic field lines are transported to the tail, where a part of them is reconnected instantaneously and convected back to the dayside magnetosphere. The enhanced convection leads to an intensification of the field aligned currents and of the high-latitude ionospheric currents. The merged magnetic field lines that are not instantaneously reconnected in the tail are added to the magnetotail lobes, contributing to the increase of the tail field and consequently to an intensification of the cross-tail current. This leads to the stretching of the magnetic field lines of the plasma sheet resulting in a more tail-like configuration. This phase is called the *substorm growth phase* and typically lasts for about one hour. The upper panel of Figure 2.12 illustrates the plasma sheet configuration during this phase.

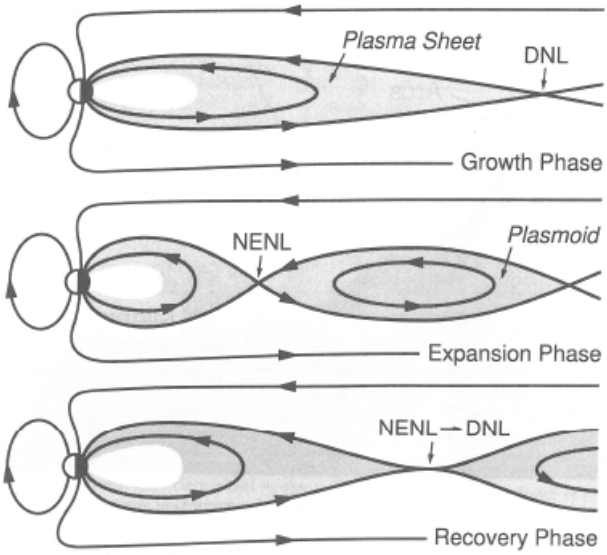

Figure 2.12: Reconfiguration of the plasma sheet during a substorm. From Baumjohann and Treumann [7].

Expansion Phase

The onset of the expansion phase is triggered by the sudden dipolarization of the stretched magnetic field lines of the plasma sheet and the consequent release of the

stored magnetic energy. The released energy energizes the plasma sheet particles that are injected into the inner magnetosphere and drift into the radiation belts. The dipolarization of the stretched magnetic field lines occurs through reconnection processes taking place in a newly formed X-line located at about 30 R_E downtail, called the *near-Earth neutral line*, NENL. In between the NENL and the *distant neutral line* (DNL) located at ~100-200 R_E, a region is formed where the magnetic field lines are neither connected to the geomagnetic field nor to the IMF, but instead form closed loops, constituting a *plasmoid*. The substorm expansion phase lasts typically between 30 to 60 minutes. The middle panel of Figure 2.12 illustrates the changes occurring in the magnetosphere during this phase.

Recovery Phase

The recovery phase is characterized by the return of the magnetosphere to a quiet state with an attenuation of the strong dipolar field orientation of the plasma sheet and with the end of reconnection occurring at the NENL. The NENL is thought to retreat tailward pushing the plasmoid until it is ejected from the magnetosheath to the downtail solar wind, and the NENL becomes the DNL (bottom panel of Figure 2.12).

The Auroral Substorm

The dramatic changes occurring in the magnetosphere during a magnetospheric substorm produce strong auroral activity in ionosphere by means of enhanced field-aligned currents and particle energization. During the growth phase, aurora appears as multiple thin arcs elongated in the east-west direction moving equatorward. The substorm onset leads to the *auroral break up*, with the brightening of the most equatorward auroral arcs occurring in the midnight sector and expanding poleward and westward forming a westward moving surge. This motion of the auroral brightening is called the *westward traveling surge*, WTS. The return of the magnetosphere to its quiet state during the recovery phase is accompanied by the decrease of brightness of the aurora at lower latitudes and by the reappearance of quiet arcs at higher latitudes.

The Magnetic Storm

When the IMF is southward oriented during a prolonged period of time, the coupling between the solar wind and the magnetosphere becomes strong and several major substorms may occur in a row, contributing to a substantial increase of the ring current density. This phenomenon is called *magnetic storm*. Eruptions on the Sun followed by mass ejections combined with a southward oriented IMF may also lead to magnetic storms due to the associated strong injections of plasma from the tail.

During storm-time periods the ring current intensifies significantly inducing a decrease of the intensity of the geomagnetic field inside the ring current torus. The

development of a magnetic storm may therefore be monitored by ground-based magnetometers located at equatorial latitudes that measure the disturbances of the geomagnetic field induced by the variations on the ring current density. The geomagnetic index D_{st} is defined as the instantaneous worldwide average of the horizontal component of the geomagnetic field from equatorial magnetograms from all over the world. Negative deflections of the D_{st} index reflect enhancements of the ring current density, while the increase of the D_{st} index follows from the decay of the ring current.

Chapter 3

Auroral Electrodynamics

3.1 Ionospheric Currents

Generalized Ohm's Law

The low-altitude ionosphere is characterized by a dense and partially ionized plasma where collisions with the neutral particles of the upper atmosphere are of major importance for the electrodynamics of this region. Besides the high conductivity along the magnetic field direction due to the large mobility of the electrons along this direction, the conductivity along the direction perpendicular to the magnetic field is also significant (but typically much lower), and results from the collisions between the ionospheric charged particles and the neutral atmosphere.

Let us consider a particle with charge q moving with velocity $\mathbf{v}$ under the action of the Coulomb and Lorentz forces . Assuming that the neutral particles are at rest, and that the collision frequency with the neutral particles is ν_c , the equation of motion for the charged particles is

$$m\frac{d\mathbf{v}}{dt} = q\left(\mathbf{E} + \mathbf{v} \times \mathbf{B}\right) - m\nu_c\mathbf{v}. \tag{3.1}$$

For an electron moving with velocity $\mathbf{v}_e$ in an unmagnetized plasma in steady state, and neglecting the motion of the ions, Equation 3.1 together with $\mathbf{j} = q_e n_e \mathbf{v}_e$, results in Ohm's law

$$\mathbf{j} = \sigma_0 \mathbf{E} \tag{3.2}$$

where

$$\sigma_0 = \frac{n_e q_e^2}{m_e \nu_{ce}} \tag{3.3}$$

is the plasma conductivity, m_e and n_e are the electron mass and density, respectively, and $q_e = -e$ is the electron charge.

In a magnetized plasma such as in the ionosphere the electric field induced by the motion of the charged particle across the magnetic field must be taken into account resulting in Equation 3.4,

$$\mathbf{j} = \sigma_0 \left(\mathbf{E} + \mathbf{v} \times \mathbf{B} \right). \tag{3.4}$$

This equation is valid in rare and fully-ionized plasmas, such as the solar wind and the magnetospheric plasmas, where the collision frequency is extremely low and the conductivity is therefore near-infinite, and may be treated as a scalar, since the anisotropy introduced by the presence of a magnetic field is negligible in this case.

However, in the partially-ionized and dense ionosphere, the collision frequency is large. Consequently, the anisotropy introduced by the presence of a magnetic field results in an anisotropic conductivity, that should therefore be treated as a tensor. The equation of motion for an electron in a magnetized plasma in steady state is (from Equation 3.1)

$$\mathbf{E} + \mathbf{v}_e \times \mathbf{B} = \frac{m_e \nu_{ce}}{q_e} \mathbf{v}_e. \tag{3.5}$$

Considering $\mathbf{j} = q_e n_e \mathbf{v}_e$ and the definition of plasma conductivity (Equation 3.3), yields another form of Ohm's law

$$\mathbf{j} = \sigma_o \mathbf{E} + \frac{\sigma_0}{n_e q_e} \mathbf{j} \times \mathbf{B}. \tag{3.6}$$

This equation is equivalent to

$$\mathbf{j} = \sigma \mathbf{E}, \tag{3.7}$$

where σ is the conductivity tensor given by

$$\begin{pmatrix} \sigma_P & -\sigma_H & 0 \\ \sigma_H & \sigma_P & 0 \\ 0 & 0 & \sigma_{||} \end{pmatrix}$$

and

$$\sigma_P = \frac{\nu_{ce}^2}{\nu_{ce}^2 + \omega_{ge}^2} \sigma_0 \tag{3.8}$$

$$\sigma_H = -\frac{\omega_{ge} \nu_{ce}}{\nu_{ce}^2 + \omega_{ge}^2} \sigma_0 \tag{3.9}$$

$$\sigma_{||} = \sigma_0 = \frac{n_e q_e^2}{m_e \nu_{ce}} \tag{3.10}$$

where ω_{ge} is the electron gyro-frequency given by Equation 2.9. σ_P is the *Pedersen conductivity* that determines the *Pedersen current* flowing along the direction of

the electric field component that is perpendicular to the magnetic field, i.e., $E_\perp$. σ_H is the *Hall conductivity* responsible for the *Hall current* flowing in the direction perpendicular to both the electric and magnetic fields. The current flowing parallel to the magnetic field is determined by the *parallel conductivity*, $\sigma_{||}$.

According to these definitions, Equation 3.7 may be rewritten into the form

$$\mathbf{j} = \sigma_{||}\mathbf{E}_{||} + \sigma_P\mathbf{E}_\perp - \sigma_H\frac{(\mathbf{E}_\perp \times \mathbf{B})}{B}. \tag{3.12}$$

In the ionospheric plasma, not only the electrons but also the ions are scattered by the neutrals. In a similar way as deduced for the current carried by the electrons, Equation 3.7 may also be used to describe the current carried by the ions, with the total current being the sum of both. Hence, the total conductivity tensor has two similar terms, one referring to the electrons and the other to the ions. Since the sign of the charge is included in the definition of the cyclotron frequency (Equation 2.9), the ion contribution is simply found by replacing ω_{ge} by ω_{gi}, ν_{ce} by ν_{ci} and the plasma conductivity σ_0 (that is equivalent to the electron conductivity when neglecting the motion of the ions) by the ion conductivity σ_i. The total conductivity tensor is then given by

$$\sigma_P = \frac{\nu_{ce}^2}{\nu_{ce}^2 + \omega_{ge}^2}\sigma_e + \frac{\nu_{ci}^2}{\nu_{ci}^2 + \omega_{gi}^2}\sigma_i \tag{3.13}$$

$$\sigma_H = -\left(\frac{\omega_{ge}\nu_{ce}}{\nu_{ce}^2 + \omega_{ge}^2}\sigma_e + \frac{\omega_{gi}\nu_{ci}}{\nu_{ci}^2 + \omega_{gi}^2}\sigma_i\right). \tag{3.14}$$

$$\sigma_{||} = \sigma_e + \sigma_i = \frac{n_e q_e^2}{m_e\nu_{ce}} + \frac{n_i q_i^2}{m_i\nu_{ci}} \tag{3.15}$$

Current Closure Through the Ionosphere

The ionospheric currents flowing at auroral and higher latitudes have three distinct components, as described in Equation 3.12. Since in the Earth's geomagnetic field, the electron cyclotron frequency is much larger than the electron collision frequency ($\omega_{ge} \approx 10^7$ Hz, $\nu_{ce} \approx 10^4$ Hz at 125 km altitude), $\sigma_{||}$ is always much larger than σ_P and σ_H ($\sigma_{||} \approx 10^{-2}$ S/m, $\sigma_P \approx 9 \times 10^{-7}$ S/m, $\sigma_H \approx 7 \times 10^{-6}$ S/m, at 125 km altitude, in the nightside during solar maximum). Consequently, and in order to maintain current continuity, the electric field component perpendicular to the magnetic field ($E_\perp$) will generally be much larger than the field-aligned electric field component ($E_{||}$). Assuming that the magnetic field lines are perfectly conducting and nearly vertical at auroral and higher latitudes, the horizontal (perpendicular) component of the electric field may be considered height-independent. The height-integrated Ohm's law may be then defined as

$$\mathbf{J}_\perp = \Sigma_P \mathbf{E}_\perp - \Sigma_H \frac{(\mathbf{E}_\perp \times \mathbf{B})}{B} \tag{3.17}$$

where $\mathbf{J}_\perp$ is the height-integrated horizontal current density and Σ_P and Σ_H are the height-integrated Pedersen and Hall conductivities, respectively, also called *Pedersen and Hall conductances.*

In a stationary state, the divergence of the total current is zero. Hence, it results that

$$j_{||} = -\nabla_\perp \cdot \mathbf{J}_\perp \tag{3.18}$$

where $j_{||}$ is the density of the field-aligned current flowing upward away from the ionosphere.

By combining Equations 3.1 and 3.18, and considering that the ionospheric magnetic field is uniform in the horizontal direction on time scales of the order of the electron collision time, yields

$$j_{||} = -\left(\nabla_\perp \Sigma_P\right) \cdot \mathbf{E}_\perp + \left(\nabla_\perp \Sigma_H\right) \cdot \frac{(\mathbf{E}_\perp \times \mathbf{B})}{B} - \Sigma_P \left(\nabla_\perp \cdot \mathbf{E}_\perp\right). \tag{3.19}$$

This equation describes the coupling of the ionospheric currents flowing at auroral latitudes with the magnetosphere. It says that whenever there is a horizontal gradient of the Pedersen conductance in the horizontal direction, or a horizontal gradient of the Hall conductance in the direction perpendicular to both the horizontal electric field and the magnetic field, or a horizontal divergence of the horizontal electric field, field-aligned currents are generated connecting the ionospheric current system with the magnetosphere. However the field-aligned currents may be limited by the number of charge carriers available and/or by a possible magnetospheric current closing the circuit at high altitudes. In this case, polarization electric fields are generated that change the divergence of the electric field (third term in Equation 3.19) in order to decrease the need of large field-aligned current densities imposed by large conductivity gradients or by an intense convection electric field (two first terms of Equation 3.19).

Polarization electric fields may also be generated when the ionospheric conductivity pattern limits the intensity of the Hall current, preventing the full closure through the ionosphere of externally imposed field-aligned currents. This may occur for example in bands of enhanced ionization created by auroral arcs, as schematically illustrated in Figure 3.1.

The accumulation of opposite charges along the edges of a channel of enhanced conductivity results from the fact that the Hall current, driven by the primary electric field $\mathbf{E}_0$, is prevented from flowing outside the channel. A polarization electric field $\mathbf{E}_1$ is consequently formed and grows in intensity until its Pedersen current $\Sigma_P \mathbf{E}_1$ equals the oppositely directed Hall current $\Sigma_H \mathbf{E}_0$, which occurs when $\mathbf{E}_1 = \Sigma_H / \Sigma_P \mathbf{E}_0$. The polarization electric field $\mathbf{E}_1$ also drives a Hall current, $\Sigma_H \mathbf{E}_1$,

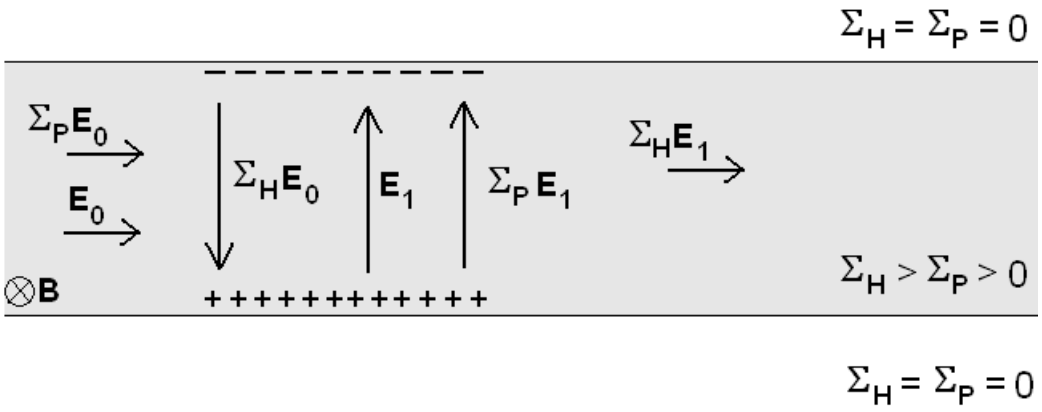

Figure 3.1: The Cowling channel.

which adds to the primary Pedersen current, $\Sigma_P \mathbf{E}_0$. The total Pedersen current is therefore equal to

$$\mathbf{J}_P^{tot} = \Sigma_P \left(1 + \frac{\Sigma_H^2}{\Sigma_P^2}\right) \mathbf{E}_0. \tag{3.20}$$

$\Sigma_P(1+\Sigma_H^2/\Sigma_P^2)$ is called the *Cowling conductivity* and can be up to 10 times larger than the Pedersen conductivity in the ionosphere.

The Auroral Oval Current System

The *auroral oval* has the shape of an oval ring centered about 3 °-5 ° from the magnetic pole toward midnight, and represents the instantaneous distribution of auroras. It is characterized by a significant ionization due to enhanced particle precipitation into this region. Figure 3.2 shows a picture of the auroral oval as seen from space, overlaid on top of a visible image of the Earth. The brightest auroras are seen in midnight and premidnight region.

Associated with the significant particle precipitation into the auroral oval, the ionospheric conductivity is enhanced in this region. The high-latitude ionospheric current flow is therefore concentrated into the auroral oval, where it forms the *auroral electrojets*. The auroral electrojets carry a total current of about 10^6 A and flow at an altitude of about 120 km above the Earth's surface [7], inducing a magnetic field disturbance at the ground level that can reach up to about 5 % of the geomagnetic dipole field during the largest magnetic storms. The disturbance field caused by the auroral electrojets may therefore be larger than that induced by the ring current flowing around the Earth.

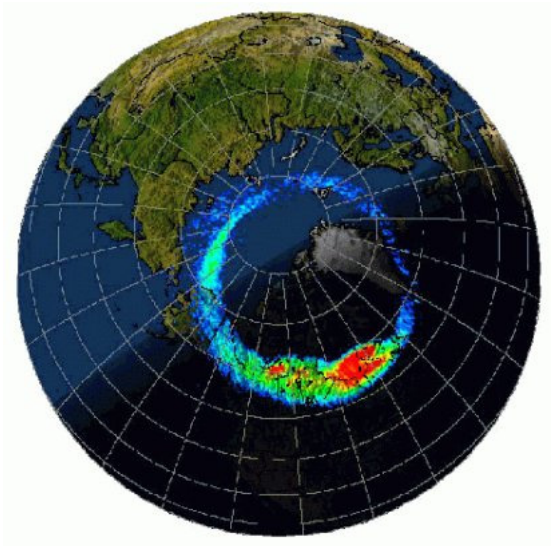

Figure 3.2: View of the auroral oval from space. Image credit: Holzworth and Meng, NSSDC, NASA

The auroral electrojet system composed of the *eastward electrojet* (EEJ) and the *westward electrojet* (WEJ), is schematically represented in the lower left panel of Figure 3.3. These are primarily Hall currents flowing perpendicular to the ionospheric convection electric field (top right panel) toward east in the evening and premidnight sectors, and westward in the morning and postmidnight sectors, with a density of about 0.5-1 A/m. The electrojet current density maximizes close to midnight due to high Hall conductance in this region (top left panel). Both electrojets diverge as upward field-aligned currents in the premidnight sector, in the so called *Harang discontinuity* region. This region is characterized by a sharp reversal of the ionospheric convection electric field from an equatorward field on the poleward side of the auroral oval field to a poleward field on the equatorward side. The Pedersen current circuit represented in the lower right panel flows parallel to the ionospheric convection electric field through the highly conductive auroral region, connecting the region-1 and region-2 Birkeland currents (Figure 2.10). The density of the ionospheric Pedersen currents is about 0.3-0.5 A/m.

Joule Heating and the AE Index

The collisions between the charged particles carrying the ionospheric currents with the neutral atmospheric particles result in the transfer of energy from the electric field driving the ionospheric currents to the atmospheric neutrals in terms of heat,

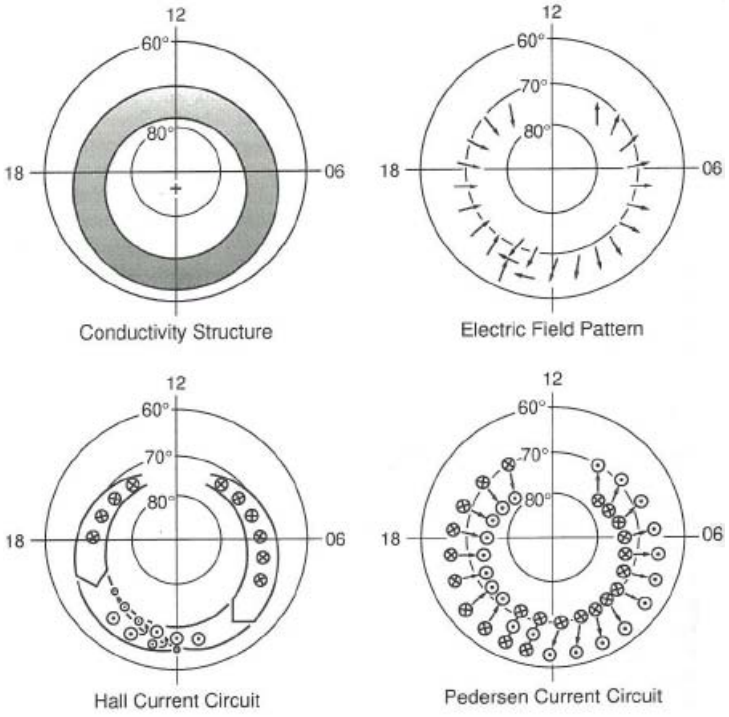

Figure 3.3: Conductivity structure, electric field pattern and Hall and Pedersen current circuits in the auroral region. From Baumjohann and Treumann [7].

i.e., energy is dissipated by *Joule heating*. The energy dissipated per unit volume and unit time integrated over the ionospheric height may be calculated from the scalar product between $\mathbf{J}_\perp$ and $\mathbf{E}_\perp$. Since the Hall current flows in the direction perpendicular to the electric field it does not contribute to the dissipation of energy. Therefore, the Joule heating rate Q_J may be written as

$$Q_J = \Sigma_P \mathbf{E}_\perp^2 \quad \left[W/m^2\right]. \tag{3.21}$$

The height-integrated Pedersen conductivity is typically about 7-10 S in the ionosphere and the ionospheric convection field about 20-50 mV/m, yielding a Joule heating rate of about 3-25 mW/m^2. A rough estimate of the total heat input into the auroral oval gives a value of $10^{10} - 10^{11}$ W (approximating the auroral oval to a ring centered on the pole and covering the latitude range 65 °-75 °).

The total heat input into the high-altitude ionosphere may also be estimated from the *AE index* which is a measure of the global electrojet activity in the auroral zone obtained from the average of the difference between the maximum poleward

and equatorward disturbance magnetic fields calculated over a number (10 to 12) of stations distributed in local time in the auroral region of the Northern Hemisphere. The maximum poleward (equatorward) disturbance magnetic field represents the maximum current density of the EEJ (WEJ) and constitutes the AU (AL) index, respectively. The AE index is equivalent to the difference AU - AL calculated at each instant. The AE index may vary from about 100 nT during weak substorm activity up to about 1000 nT or even larger during strong magnetic storms, corresponding to a total heat input of about $10^{10} - 10^{11}$ W (according to the empirical relation 1 nT in AE $\approx$ 0.3 GW).

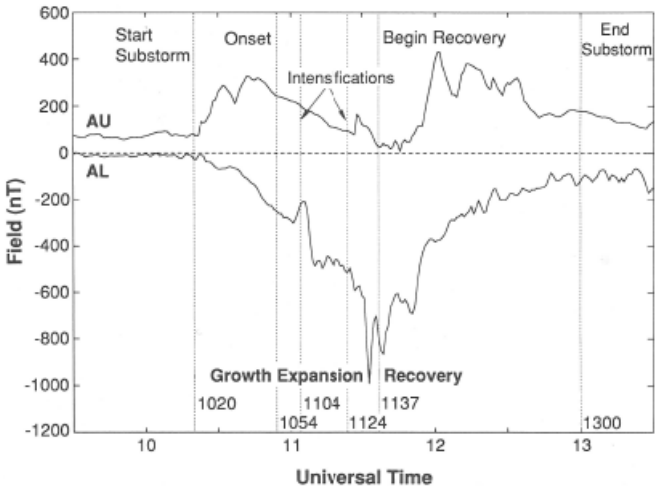

Figure 3.4: AU and AL indices for a particular substorm. From Kivelson and Russel [38].

The dependence of the ionospheric current flow on substorm activity is reflected on the auroral electrojet indices (AU, AL and AE). For this reason, their analysis constitutes a major tool for the identification of the different substorm phases. Figure 3.4 shows the AU and AL indices for a particular substorm. The different substorm phases are indicated at the bottom of the figure. A clear departure from the background level associated with quiet-time conditions identifies the start of the substorm growth phase. The onset (beginning of the expansion phase) separates a period of slowly growing indices from a period characterized by faster variations. After reaching the peak of the expansion phase, the growth phase begins with the decrease of the AL index and the return to the background level.

3.2 The Auroral Current Circuit

Figure 3.5 shows a schematic illustration of the lower part of the *auroral current circuit*. It typically consists of a region of downward flowing field-aligned currents carried mainly by ionospheric electrons moving upward along the magnetic field lines. This region is called the *downward* or *return current region*. Horizontal ionospheric currents flowing perpendicular to the magnetic field connect the downward current with the *upward* or *primary current* which is carried by downward moving electrons of magnetospheric origin.

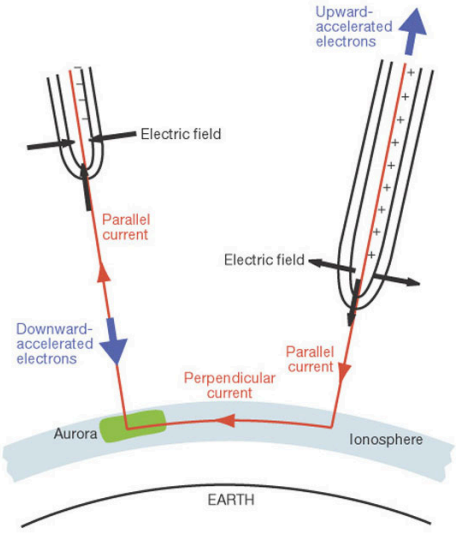

Figure 3.5: Schematic illustration of the auroral current circuit. From Marklund *et al.* [44].

The existence of electric fields parallel to the background magnetic field in the upward current region was theoretically postulated by Hannes Alfvén [1] about 50 years ago. Alfvén's prediction was experimentally confirmed some years later by measurements of monoenergetic peaks in the electron spectra made on board a sounding rocket [48], and of narrow beams of fast upflowing O+ ions detected at $\sim$1 R_E on board the S3-3 satellite [63]. The formation of field-aligned electric fields is linked to the requirement of current continuity, when the number of charge carriers is limited, which is often the case on auroral field lines at high altitudes. In the case of the upward current region represented on the left side of Figure 3.5, the downward moving electrons are accelerated in the parallel downward direction and may gain energies up to tens of keV (e.g. Paper 2 and Paper 3). The pitch-angle of the accelerated electrons decreases (electrons become more field-aligned),

and they may therefore be lost into the upper atmosphere where their energy is dissipated through collisions with the neutrals powering in this way the display of light emissions.

Parallel electric fields in the auroral region were thought to occur only in the upward current region. However, Marklund *et al.* [42] presented results from the Swedish satellite Freja showing diverging electric fields, perpendicular to the background magnetic field, associated with the absence of auroral emissions. These observations imply the existence of a field-aligned electric field located below the spacecraft that accelerates the electrons in the upward field-aligned direction reaching energies of up to 3 keV [28] (right side of Figure 3.5). The configuration of the potential structures observed in the upward and downward current regions, is further discussed in the next section.

The main results of several studies ([39, 40, 57, 42, 43, 47, 51, 78], and references therein) performed during the last four decades on the upward and downward current regions are summarized below (Table 3.1).

Upward current region (UCR)	Downward current region (DCR)
Acc. region typically located between 2000 km and 2 R_E altitude	Acc. region located between 1000 and 4000 km altitude
The acc. region extends to higher altitudes during Summer	The acc. region extends to higher altitudes during Summer
Converging electric fields structures	Diverging electric fields structures
Downgoing field-aligned electrons	Upgoing field-aligned electrons
Upgoing ion beams and ion conics	Ion heating transverse to B - formation of energetic ion conics
Current-voltage relation is relatively well understood (Knight relation) $j_{\|\|}=K\cdot\Delta\Phi_{\|\|}$, $K=\frac{e^2 n}{\sqrt{2\pi m_e k_B T_e}}$	Current-voltage relation remains unclear. Current density is a few times larger than in the UCR for similar $\Delta\Phi_{\|\|}$
Narrow ($\sim$10 km) fingers of potential extending along the magnetic field are seen at the bottom of the acc. region	

Table 3.1: Main characteristics of the upward and downward current acceleration regions.

A third region characterized by parallel acceleration of particles by wave electric fields is located close to the nightside polar cap boundary, known as the *Alfvénic region*. This region is characterized by filamentary Alfvénic currents with no preferred sense, by intense low-energy ion outflow and by downward moving electrons strongly accelerated in the parallel direction by Alfvén waves responsible for some of the brightest aurora in the midnight region. The propagation of Alfvén waves along the magnetic field lines threading the nightside polar cap boundary is thought to occur in order to achieve a convective equilibrium between the magnetospheric and the ionospheric plasmas, in the recently reconnected field lines that map to the nightside polar cap boundary.

3.3 Field-Aligned Potential Structures and Coupling to the Ionosphere

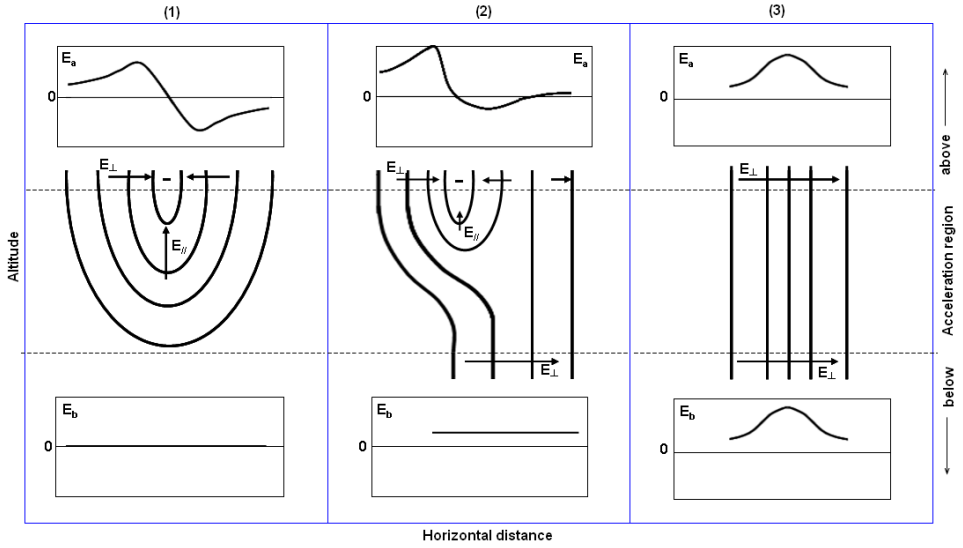

Figure 3.6: Schematic drawing of the equipotentials of three high-altitude electric field structures in the upward current region corresponding to (1) a total decoupling from the ionosphere, (2) a partial coupling and (3) a total coupling with the ionosphere. The electric field profiles observed when crossing above (E_a) and below (E_b) the corresponding acceleration regions are shown at the top and bottom of each panel, respectively.

Figure 3.6 shows the equipotentials corresponding to three different configurations of electric field structures in the upward current region. The electric field

profiles observed when crossing above and below the acceleration regions (along the horizontal dashed lines) of each case are schematically represented at the top (E_a) and at the bottom (E_b) of each panel.

Panel (1) shows the case of a pure *U-shaped potential structure* [11], where the equipotentials close above the ionosphere, and hence the potential structure is totally decoupled from the low ionosphere. The combination of a U-shaped potential structure with a constant ionospheric electric field results in the structure represented in panel (2). This case corresponds to a partial coupling with the ionosphere, where some equipotentials close above the ionosphere while others are linked to the ionosphere, forming a *S-shaped potential structure* [43]. In panel (3) is represented the case of a local enhancement of the electric field that maps perfectly along the magnetic field lines, corresponding to a perfect magnetosphere-ionosphere coupling. For simplicity reasons, the magnetic field lines are here considered to be parallel. In reality the magnetic field lines converge toward lower altitudes, and therefore the electric field magnitude mapped along a magnetic field line increases with decreasing altitude. The three cases represented in Figure 3.6 apply equally well to the downward current region, with the potential structures having the opposite sign and the electric fields pointing in the reverse direction.

The nearly symmetric divergent electric fields associated with dropouts of precipitating electrons observed by Marklund *et al.* [42, 43], and the nearly symmetric convergent electric field structures shown in Papers 2 and 3 of this thesis, are examples of positive and negative U-shaped potential structures typically observed in the downward and upward current regions, respectively. The asymmetric electric fields associated with upward accelerated electrons observed in the downward current region [28], and with upward accelerated ions in the upward current region (Paper 3 of this thesis), are examples of typical positive and negative quasi-static S-shaped potential structures, respectively. Being quasi-static implies that the structures are steady over a time frame within which a particle traverses the acceleration region without experiencing a significant change of the total potential [9].

A distribution of the characteristic energy of field-aligned moving particles when plotted as a function of time, resembling the Greek letter Λ, is normally designated as an inverted-V distribution. The energy of the particles is larger in the center and falls off at the edges. This corresponds to the energy distribution of particles that have been accelerated in the field-aligned direction when moving through a U-shaped potential structure. The particles accelerated in the centre of the potential structure gain more energy than those accelerated at the edges. The observation of such a signature in the energy spectrogram of downgoing electrons indicates the existence of negative U-shaped equipotentials above the spacecraft, as in the case reported in Paper 2 of this thesis. The observation of upgoing inverted-V ions/electrons in the upward/downward current region points to the existence of a negative/positive U-shaped potential structure below the spacecraft accelerating the ions/electrons upward away from the ionosphere along the magnetic field direction.

Hwang *et al.* [26] used data from the FAST satellite to study electric field

structures in the return current region. They used the ratio between the potential at the spacecraft and the upgoing electron characteristic energy as a measure of the coupling degree of a potential structure to the low ionosphere. They showed that the degree of coupling is related to the morphology of the structure: curved structures are associated with potential structures mainly decoupled from the ionosphere and generated by a high-altitude source, while sheetlike structures such as straight arcs are associated with potential structures that are mainly coupled to the ionosphere, having a contribution of an ionospheric electric field. The generation of high-amplitude, small-scale, ionospheric electric fields can occur as the response to an externally applied downward field-aligned current. The evacuation of ionospheric electrons by the downward field-aligned current decreases the ionospheric Pedersen conductivity requiring large perpendicular electric fields in order to maintain current continuity. On the other side, limitations of the number of charge carriers of the downward current require the formation of a potential structure at higher altitudes that accelerates the electrons along the field-aligned direction to maintain the required current density. Ionospheric feedback plays in this case an important role for the formation of intense perpendicular electric field structures at higher altitudes [41, 71].

Hwang also found that sheetlike structures show typically upgoing Poynting fluxes, while curved structures are mainly associated with downgoing Poynting fluxes. The field-aligned transport of electromagnetic energy by upward propagating Alfvén waves (in the form of upward-directed Poynting flux) is associated with the upward propagation of the information about changes occurring in the ionosphere. The free energy carried by the upward moving Alfvén waves may have many different causes, as for example a local reduction of the Joule heating [41].

The coupling of magnetospheric perpendicular potentials to the ionosphere has been seen to depend also on the perpendicular width of the structure in the ionosphere ($w_{\perp ion}$) and on the *coupling scale length*, $L = \sqrt{\frac{\Sigma_G \Sigma_P}{K(\Sigma_G + \Sigma_P)}}$, where Σ_P is the height-integrated Pedersen conductivity, Σ_G is the height-integrated generator conductivity, and K is the constant of proportionality in the current-voltage relationship of the upward current region (Table 3.1) [54]. In the model of a voltage generator (low internal resistance), $\Sigma_G >> \Sigma_P$, and the coupling scale length becomes $\sqrt{\frac{\Sigma_P}{K}}$, generally designated as λ_{ES}. In the case of a current generator (high internal resistance), $\Sigma_G << \Sigma_P$, and therefore the coupling scale length is $\sqrt{\frac{\Sigma_G}{K}}$. If $w_{\perp ion} << L$, the magnetospheric potential structures are decoupled from the ionosphere, while $w_{\perp ion} >> L$ favors a coupling of the high-altude potential structures to the low ionosphere. Since $\sqrt{\frac{\Sigma_G}{K}}$ is generally smaller than $\sqrt{\frac{\Sigma_P}{K}}$, current generators are more likely associated with the formation of small-scale structures than voltage generators. For typical values of Σ_P and K, the coupling scale length is, for the case of a voltage generator, about 100 km. For the case of a current generator, and assuming $\Sigma_G = 0.01\Sigma_P$, the coupling scale length is about 10 km.

3.4 Auroral Acceleration by Alfvén Waves

Alfvén waves occur throughout the auroral oval but are more common near the polar cusps and the polar cap boundary near midnight where they can power bright aurora [84].

Alfvén waves are electromagnetic waves propagating in conductive fluids along the direction of the background magnetic field $\mathbf{B}_0$, with a frequency less that the ion gyrofrequency, $\omega_{ci} = q_i B_0/m_i$. Their existence was predicted by Alfvén in 1942 [2]. The dispersion relation for an Alfvén wave propagating in the direction parallel to a homogeneous magnetic field $\mathbf{B}_0$ is given by

$$\omega = V_A k_{||} \tag{3.22}$$

where $k_{||}$ is the component of the wave vector $\mathbf{k}$ along the magnetic field direction, and V_A is the Alfvén velocity given by

$$V_A = \frac{B_0}{\sqrt{\mu_0 \rho}}, \tag{3.23}$$

where μ_0 is the permeability of vacuum and ρ is the mass density.

In the case of a quasi-stationary current system ($\nabla \cdot \mathbf{j}=0$, Section 3.1) with infinite extension in the y-direction, it may be shown that

$$\frac{E_x}{b_y} = \pm \frac{1}{\mu_0 \sum_P}, \tag{3.24}$$

where $\sum_P$ is the Pedersen conductance, $\mathbf{E}$ is the electric field and $\mathbf{b}$ is the perturbation magnetic field. The +(-) sign refers to the Northern (Southern) hemisphere, respectively.

A similar relation may be deduced for the case of an Alvén wave in ideal MHD

$$\frac{E_\perp}{b} = \pm V_A = \pm \frac{1}{\mu_0 \Sigma_A}, \tag{3.25}$$

where $E_\perp$ is the electric field component perpendicular to the direction of propagation, Σ_A is the Alfvén conductance and the +(-) sign applies for propagation parallel (anti-parallel) to $\mathbf{B}_0$, respectively. Also here, $\mathbf{b}$ represents the perturbation magnetic field.

The comparison of the quantity $\mu_0 \frac{E_x}{b_y}$ with the inverse of the Pedersen and Alfvén conductances is a method for distinguishing between the quasi-static structures described in the previous section and temporal variations associated with Alfvén waves. Since the Alfvén velocity can vary significantly along an auroral field line (from a few hundred kilometers per second in the ionosphere, up to over 100 000 km/s in the auroral acceleration region at 4000-6000 km altitude and then decreasing to the 1000 km/s range at higher altitudes), Σ_A varies typically between 0.01 S up to 1.0 S. Σ_P is typically in the 1-10 S range, which results in generally larger values of the ratio $\mu_0 \frac{E_x}{b_y}$ for Alfvén waves than for quasi-static structures.

The dispersion relation for an Alfvén wave in the ideal MHD limit (Equation 3.22) implies that both the phase and the group velocities are equal to the Alfvén velocity and do not depend on the wavelengths parallel or transverse to the magnetic field. The wave is therefore not dispersive: all frequencies travel at the same velocity. Another important property of the Alfvén waves in ideal MHD is that the parallel component of the electric field of the wave is zero. In the real case when the Alfvén wave has a small perpendicular wavelength, effects of electron inertia and thermal effects must be taken into account, resulting in the dispersion of the Alfvén waves and in the generation of an electric field parallel to the magnetic field, which can accelerate particles.

In the low-temperature plasma of the topside ionosphere where the electron thermal speed is below the Alfvén speed, the effects of electron inertia dominate and therefore the *inertial Alfvén wave* is the most common Alfvénic wave mode. The dispersion relation is in this particular case given by

$$\omega = k_{||} \frac{V_A}{\sqrt{1 + k_\perp^2 \lambda_e^2}} \tag{3.26}$$

where λ_e=c/ω_{pe} is the electron inertial length or electron skin depth, c is the speed of light in vacuum, ω_{pe} is the angular plasma frequency $\left(\omega_{pe} = \sqrt{\frac{n_e e^2}{m_e \epsilon_0}}\right)$, and $k_\perp$ is the perpendicular component of the wave vector.

At altitudes above ~2 R_E the electron thermal velocity becomes larger than the Alfvén velocity and the thermal effects dominate. In this case, the *kinetic Alfvén wave* is the dominant wave mode. The dispersion relation is in this case

$$\omega = k_{||} V_A \sqrt{1 + k_\perp^2 \rho_s^2} \tag{3.27}$$

with ρ_s=$\sqrt{T_e/m_i}/\omega_{ci}$ being the ion gyroradius at electron temperature.

Both the inertial and the kinetic Alfvén wave modes become dispersive at small scales, and the ratio $\frac{E_\perp}{b}$ (Equation 3.25) becomes dependent on the transverse wavevector.

The generation of a parallel electric field caused by finite-$\lambda_\perp$ effects and carried by the propagating inertial and kinetic Alfvén wave modes leads to the exchange of momentum and energy with the plasma resulting in significant heating of the plasma and field-aligned acceleration of electrons.

Several studies have shown that the electromagnetic energy carried by the Alfvén waves in the form of Poynting flux ($\mathbf{S}$=$\frac{\mathbf{E}\times\mathbf{b}}{\mu_0}$) powers the downward acceleration of electrons at high altitudes resulting in the formation of very bright aurora [12]. Irregularities such as density gradients and changes in the plasma flow associated with reconnection processes occurring in the magnetosphere are sources of energy for the Poynting flux carried by the Alfvén waves into the ionosphere. Observations from the Polar satellite showed cases where the perpendicular electric fields observed in the PSBL at 4-6 R_E altitude were associated with Alfvén waves with sufficient Poynting flux to generate intense auroral structures [84, 32]. Moreover,

large Poynting fluxes exceeding 100 mW/m^2 when mapped to the ionosphere were observed magnetically conjugate with intense auroral emissions, demonstrating the important role that Alfvén waves have in the acceleration of auroral particles in the PSBL region. Keiling *et al.* [33] showed that the Alfvén wave Poynting flux contributes with about 30-35 % of the total energy flux powering the ionospheric aurora, with the large-scale field-aligned currents being the main contributor.

3.5 The Aurora

Precipitating particles that reach down to the upper atmosphere (∼100 km altitude) will collide and excite neutral atoms and molecules. The emission of light of certain wavelenghts resultant from the de-excitation of the excited particles gives origin to magnificent auroral displays (Figure 3.7).

Figure 3.7: A beautiful auroral display over Alaska. Image credit: H. Dahlgren.

The aurora may be classified into three main categories according to the associated acceleration mechanism. These are the *discrete aurora*, the *black aurora* and the *diffuse aurora*. The main characteristics of each of these categories is described below.

Discrete aurora

The discrete auroras are associated with intense auroral emissions caused by precipitating particles that have been accelerated by negative quasi-static potential drops of 5-10 kV or by Alfvén waves. They are associated with upward field-aligned currents and hence the brightest discrete auroras are found on the poleward side of

the evening and premidnight auroral oval (where the upward region-1 is located). This region is magnetically connected to the plasma sheet boundary layer. Discrete auroras are often structured and appear generally as long east-west aligned arcs but may also form spirals, curls, or folds. Figure 3.8 shows an image of a structured discrete auroral arc from the ASK (Auroral Structure and Kinetics) imager located in Tromsø taken at 02:18:10 UT on 15 December 2006.

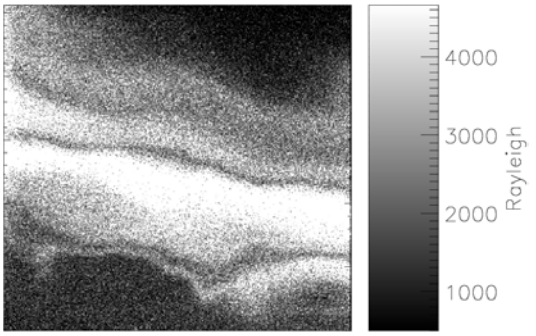

Figure 3.8: Image of multiple discrete auroral arcs from the ASK imager located in Tromsø taken at 02:18:10 UT on 15 December 2006. Courtesy of H. Dahlgren.

Black aurora

The black auroras are characterized by a lack of auroral emission often seen in a small and well-defined region within a diffuse background or intermediate between diffuse and discrete auroras [37]. They appear as east-west aligned arcs or filaments often in the evening and morning sectors, and may also develop into curls, patches or rings. The black auroral arcs have scale-sizes of 100 m to 5 km [74] similar to the thin auroral discrete arcs. The black auroras formed adjacent to discrete auroras are most probably associated with the reverse process causing discrete auroras. They result from the upward acceleration of ionospheric electrons by positive quasi-static potential structures of 0.1-3 kV [43]. Figure 3.9 shows on the left a schematic representation of a negative potential structure accelerating the electrons downward and producing the discrete aurora and a positive potential structure accelerating the ionospheric electrons upwards forming the black aurora. On the right side of the figure is a picture showing a black auroral arc in between two discrete arcs.

Diffuse aurora

Diffuse auroras occur at any local time sector of the auroral oval, but is most common found in the postmidnight sector. They are characterized by a wide band of diffuse auroral emissions without significant embedded structure, and are caused

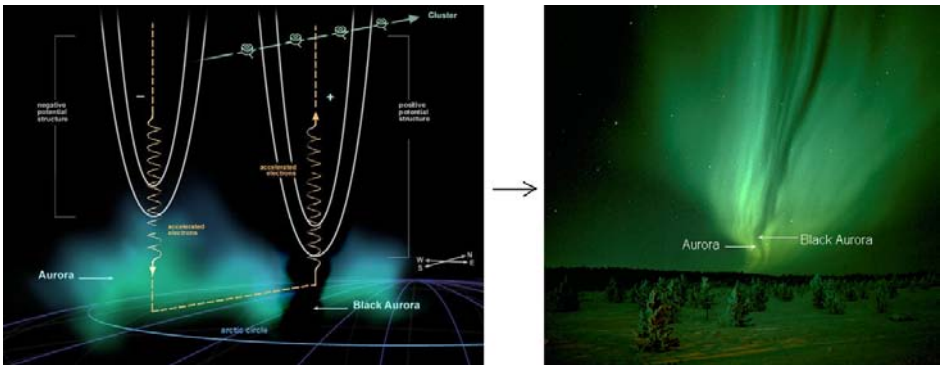

Figure 3.9: Black auroral arc in between two discrete auroral arcs. Adapted from ESA (left picture) and T. Lövgren (right picture).

by non-accelerated precipitating particles. The diffuse auroras occur at the footpoints of field lines mapping to the inner plasma sheet where the magnetic field is almost dipolar. By comparing electron energy fluxes at low altitudes with those at magnetically conjugate locations in the near-equatorial region, Schumaker *et al.* [61] confirmed that there is very little field-aligned acceleration in the quasi-dipolar region of the inner magnetosphere. The mechanism responsible for the precipitation of the particles into the diffuse auroral region is not fully understood [8]. An image of diffuse aurora from the ASK imager located in Tromsø at 20:51:04 UT on 22 October 2006 is shown in Figure 3.10. A black auroral arc is seen embedded in the region of diffuse aurora.

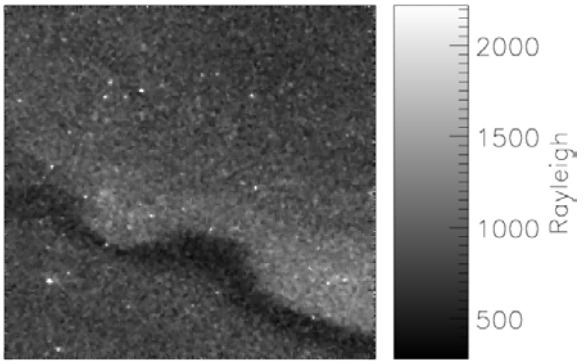

Figure 3.10: Image of a black auroral arc embedded in diffuse aurora from the ASK imager at 20:51:04 UT on 22 October 2006 in Tromsø. Courtesy of H. Dahlgren.

Chapter 4

Electric Fields in the Subauroral Ionosphere

4.1 Subauroral Ion Drifts

A common manifestation of the coupling between the magnetosphere and the ionosphere observed equatorward of the auroral oval are narrow bands of rapid westward ion flows located in the evening and postmidnight sectors. This phenomenon was first reported by Y. Galperin [20] and named *polarization jets*, PJ. The same phenomenon was later independently identified by american researchers [66, 64, 67] and termed *subauroral ion drifts*, SAID. Several studies have been carried out during the last three decades attempting to characterize the SAID phenomenon and to explain its generation mechanism. The typical characteristics of SAID events are summarized in Table 4.1.

Several generation mechanism have been proposed to explain the formation of subauroral electric fields. D. J. Southwood [65] concluded that enhanced midlatitude east-west flows may occur equatorward of the auroral oval as the result of current closure through the strong conductivity gradient at the equatorward edge of the plasma sheet electron precipitation (equatorward edge of the diffuse aurora), combined with a strong low-latitude shielding of the convection, whenever the inner edges of the ion plasma sheet and of the electron plasma sheet are close but not coincident. This model is based on the assumption that the ionospheric mapping of the ion plasma sheet inner edge is located equatorward of the auroral conductivity discontinuity, to where the inner edge of the electron plasma sheet maps. Furthermore, it is considered that the ion plasma sheet totally shields the convection electric field from lower L values. These conditions are restricted to the premidnight sector, where the plasma sheet positive ions penetrate deeper into the inner magnetosphere than the plasma sheet electrons.

Main characteristics of SAID	References
Westward ion drifts with velocities greater than 500 m/s, but most commonly greater than 1000 m/s, and reaching values up to 10 km/s.	[64], [67], [4], [60], [21], [31], Paper 1
Associated with poleward directed electric fields with amplitudes greater than 25-30 mV/m. SAID have also been termed *subauroral electric fields*, SAEF.	[64], [45], [55], [31], Paper 1
Located equatorward of the nightside auroral oval and poleward or in the vicinity of the ionospheric projection of the plasmapause.	[55], [4], Paper 1, [64], [56]
Occur predominantly in the 18-02 magnetic local time sector.	[67], [31], Paper 1
Are often detected during the substorm recovery phase, although not all are associated with substorm activity.	[46], [59],[3], [31], Paper 1
Often accompanied by ionospheric density troughs.	[24], [64], [45], [60], Paper 1
Tend to be more intense and to move towards lower latitudes with increasing magnetic activity (Kp index).	[31], Paper 1
Often located on the equatorward edge of the region-2 Birkeland currents.	[59], [4], Paper 1
Observed at conjugate locations in the Northern and Southern Hemispheres.	[59], [56]
Associated with high ion temperatures in the F-region, while no significant variations are seen in the electron temperature.	[49], [3]
Sometimes accompanied by a vertical upward flow.	[4]
Life times in the range 30 minutes to 3 hours.	[3]

Table 4.1: Typical characteristics of SAID. All velocities and electric field values refer to the topside ionosphere (∼1000 km altitude).

Anderson *et al.* [4, 3] used measurements from low-altitude orbiting satellites to study the ionospheric signatures of SAID. They suggested that the poleward electric field associated with SAID is generated as the result of current closure of the region-2 downward FACs with the region-1 upward FACs in the dusk-premidnight sector, by means of ionospheric Pedersen currents flowing through the low conductivity region of the midlatitude trough. This would most probably occur during the recovery phase of susbtorms, when the region-2 downward FACs expands to subauroral latitudes, and therefore the closing Pedersen currents flow through the low conductivity region of the midlatitude trough.

Anderson *et al.* also showed that there is always a trough associated with SAID events at altitudes near the peak of the F-region ($\sim$ 300 km), while at altitudes above 700 km the trough signature is almost absent. Furthermore, the SAID were seen to collocate with the poleward edge of a preexisting ionospheric trough, presumably formed by plasma stagnation in the region of the Harang discontinuity (described in Section 3.1), with the SAID subsequently deepening the preexisting trough. This result is in accordance with the conclusions reported earlier by Schunk and Banks [62], who investigated on the effect of rapid ion flow on the F-region chemistry. They concluded that the increase of the relative velocity between the drifting ions and the neutrals results in the increase of the reaction rate of $O^+ + N_2 = NO^+ + N$. Consequently, and due to the rapid recombination rate of NO^+, the region of fast SAID flow is expected to be characterized by a reduced ion concentration, and therefore to be associated with the formation of a trough. The reduced conductivity in the trough region leads to the further strengthening of the SAID electric field, in order to maintain current continuity. Anderson *et al.* [4] therefore concluded that the ionospheric response is also important for the generation of very rapid SAID.

SAID may also cause the formation of plasma depletions in the outer plasmasphere during periods of high magnetic activity. This was demonstrated by Ober and Horwitz [53] using a simulation model of the evolution of the plasmasphere during a period of enhanced convection electric field, associated with a magnetospheric storm . Imposing a SAID event in the premidnight sector during the last 30 minutes of the period of enhanced convection, led to the formation of a plasma density trough embedded in the dusk bulge region of the plasmasphere. The formation of the trough resulted from the convection of low density plasma from the plasma sheet into the dusk plasmaspheric region.

De Keyser *et al.* [35, 14] argued against the mechanism proposed by Anderson *et al.*. They considered that the Anderson's mechanism can not explain why two or more SAID can be present at the same time at different latitudes, as shown to occur by Spiro *et al.* [67]. De Keyser proposed instead that intense radial electric fields may be generated by a thermoelectric effect resulting from the strong temperature gradient across the interface between the cold plasmaspheric trough and hot plasma from the plasma sheet injected at substorm onset. Based on numerical simulations, De Keyser showed that the different Larmor radius of the cold particles of the trough and of the hot plasma sheet particles generate a polarization electric field at

this interface, that maps to the ionosphere as a poleward-directed electric field. The additional consideration of the azimuthal flow shear between the partially corotating plasma trough (drifting eastward) and the injected plasma, that due to collective effects does not follow the trajectories of individual charged particles but instead drifts westward in the premidnight sector and eastward in the post-midnight sector, explains the higher occurrence probability of SAID in the premidnight sector: the electric field associated with the convecting plasma in the evening sector adds to the thermoelectric field, while it suppresses the thermoelectric field in the postmidnight sector.

The strong coupling between the magnetosphere and the ionosphere at subauroral latitudes was emphasized in a recent study by Puhl-Quinn *et al.* [56], who presented magnetically conjugate observations of a SAID event using data from the Cluster and the DMSP (Defense Meteorological Satellites Program) F16A satellites, separated by a field-aligned distance of $\sim$4.4 R_E. The large-scale features characterizing the SAID event, such as the latitudinal width and the strength and direction of the associated field-aligned current, were common to both the magnetospheric and the ionospheric observations. However, clear differences in density substructure indicated a less effective magnetosphere-ionosphere coupling at smaller-scales.

Paper 1 of this thesis presents statistical results on the occurrence of SAID. A summary of these results is described in Chapter 6.

4.2 Subauroral Polarization Streams

While it is generally accepted that SAID are associated with substorms, several studies [85, 19, 52] have shown that intense subauroral electric fields may also occur during very strong magnetic storms. Using radar data taken over two solar cycles (1979-2000), Foster and Vo [19] found a persistent latitudinal broad region of westward flow located just equatorward of the auroral zone, extending from the dusk to the early morning sector for all Kp values greater than 4. These broad regions of westward plasma flow seen at subauroral latitudes were termed *Subauroral Polarization Streams*, SAPS. SAPS have a peak flow velocity greater than 900 m/s, are observed at invariant latitudes lower than $\sim$60 $^\circ$ and are 3 $^\circ$-5 $^\circ$ of latitude broad in the premidnight sector, while they are somewhat slower (up to 400m/s), thinner ($\sim$3 $^\circ$ of latitude broad) and are located equatorward of $\sim$55 $^\circ$ invariant latitude in the predawn sector. The term SAPS is nowadays also used by some authors as to include the narrower and more intense SAID channels, which are sometimes superimposed as smaller-scale features on the SAPS structures.

4.3 Abnormal Subauroral Ion Drifts

A new phenomenon observed equatorward of the auroral oval has recently been reported by Voiculescu and Roth [79] based on observations from the DMSP F15 satellite moving at an altitude of about 840 km. It consists of an equatorward-

directed electric field associated with a narrow channel ($1^\circ - 2^\circ$ latitude broad) of strong eastward ion drift, with speed greater than 1 km/s, occurring in the subauroral region. Voiculescu and Roth termed this phenomenon *Abnormal Subauroral Ion Drift*, ASAID. It has very similar characteristics to SAID, but inversed electric field/plasma flow direction.

Two ASAID events observed in the 20-21.5 MLT interval were presented by Voiculescu and Roth [79]. Both cases were accompanied by upward flows of ions with a speed of the same order as the zonal ion drift and coincided with deep narrow troughs in the total ion density at DMSP altitudes (850 km) and in the F-region of the ionosphere. However the cause-effect relationship between the ASAID and the F-region trough was not possible to establish. The ASAID events were associated with significant increases of the electron temperature while the ion temperature showed no significant variation. Both cases occurred during weak substorm activity and were associated with regions of very weak downward field-aligned currents. The ion zonal velocity was seen to reverse after a period of 9-12 hours, turning the events into classical SAID events.

From the analysis of particle data, Voiculescu and Roth concluded that the ASAID events were magnetically connected to the region just outside the plasmasphere, very near the plasmapause. They considered that the associated equatorward directed electric fields result from finite Larmor radius effects at the interface between the hot ring current and the cold plasma trough, when the outer edge of the ring current coincides with the plasmapause. The larger Larmor radius of the hot ring current ions creates an excess of positive charges in the cold plasmaspheric trough region, that generates a polarization electric field pointing radially inward (toward magnetic shells with lower L-values), and mapping down to the subauroral ionosphere as an equatorward-directed electric field. The ionospheric particles will consequently $\mathbf{E}\times\mathbf{B}$ drift in the eastward direction. The observed ASAID/SAID turning was suggested to occur when energetic electrons from the plasma sheet came close enough to the ion sheet associated with the ASAID, to generate an outward-directed polarization electric field that maps down to the subauroral ionosphere as a poleward-directed electric field.

Ionospheric eastward plasma flows observed in the midlatitude region have in fact also been reported earlier by Ebihara *et al.* [16]. Based on two-dimensional radar observations, two eastward flow events were identified in the predusk subauroral region (between 14.5 and 16 MLT). The observed channels of eastward plasma flow were about $\sim 3^\circ$ latitude broad, and the drift velocities were considerably slower ($\sim$50-70 m/s) compared to the observations by Voiculescu and Roth [79]. These events occurred during an intense magnetic storm, as SAPS typically do.

Ebihara interpreted the appearance of eastward plasma drifts in the subauroral region as a consequence of overshielding of the ionospheric dawn-dusk convection electric field by a more intense and oppositely directed electric field associated with the closure of the region-2 Birkeland currents in the dusk-dawn direction. As referred in Section 2.5, overshielding may happen when a sudden northward turning

of the IMF occurs after a prolonged period of southward-directed IMF. The magnitude of the convection electric field decreases rapidly but the pressure gradients that generate the region-2 Birkeland currents remain strong for a while. A dusk-dawn oriented Pedersen electric field still exists in the low conductivity subauroral region driving the closure of the region-2 current system, and becomes more intense than the weakened dawn-dusk convection electric field. Hence, overshielding occurs leading to antisunward flow in the predusk region.

However, while overshielding due to a sudden northward turning of the IMF may explain one of the events reported by Ebihara, it can not explain the other event observed during a period of southward-directed IMF. Ebihara argues that the shielding electric field may however still overcome the convection electric field, if the polar cap shrinks while the cross-polar cap potential drop is maintained constant, or if a sudden injection of hot ions from the nightside plasma sheet generates an inertial current flowing westward that diverts into a field-aligned current flowing into the ionosphere and closing in the dusk-dawn direction, enhancing in this way the shielding electric field. However neither of these alternatives was shown to fully account for the observations.

The Paper 4 of this thesis reports on the first statistical results on ASAID occurrence. A summary of these results is presented in Chapter 6.

Chapter 5

Instrumentation and Data Handling

5.1 The Astrid-2 Spacecraft

Astrid-2 was a Swedish micro-satellite built with the scientific objective of diagnosing auroral electrodynamics in the Earth's ionosphere and upper atmosphere. In addition it had the technological objective of demonstrating the feasibility of using micro-satellites for space research.

The Astrid-2 satellite was launched on 10 December 1998 and remained operational until 24 July 1999 when a failure of the telemetry system occurred. The spacecraft was placed in a circular orbit at 1000 km altitude, with 83° inclination and an orbital period of 105 minutes. The orbital plane regressed 180° relative to the Sun in approximately 4 months, allowing the coverage of all local times during the life time of the spacecraft. The spacecraft was spin-stabilized with a spin period of 6 seconds.

The small dimensions of the spacecraft platform ($45 \times 45 \times 30$ cm) was possible due to the development of new technology that resulted in scientific instruments with considerable reduced weight and size. The mass of the scientific payload was only $\sim$10 kg and carried EMMA, the instrument for the Electric and Magnetic Monitoring of the Aurora, LINDA, the Langmuir INterferometry and Density experiment for Astrid-2, MEDUSA, a Miniaturized Electrostatic DUal-tophat Spherical Analyzer, PIA, a Photometer for Imaging the Aurora, and ASC, an Advanced Stellar Compass. Figure 5.1 shows the location of the instruments on-board the Astrid-2 platform.

The electric and magnetic field data used in Papers 1 and 4 of this thesis are measurements from the EMMA instrument. The EMMA instrument was designed to provide simultaneous sampling of the two spin plane components of the electric field and the full magnetic field vector with variable time resolution. The electric field components were measured by two pairs of opposing probes mounted on wire booms in the spin plane of the satellite. Thus the electric field component along the spin axis was not measured, but can be calculated using the assumption $\mathbf{E} \cdot \mathbf{B} = 0$.

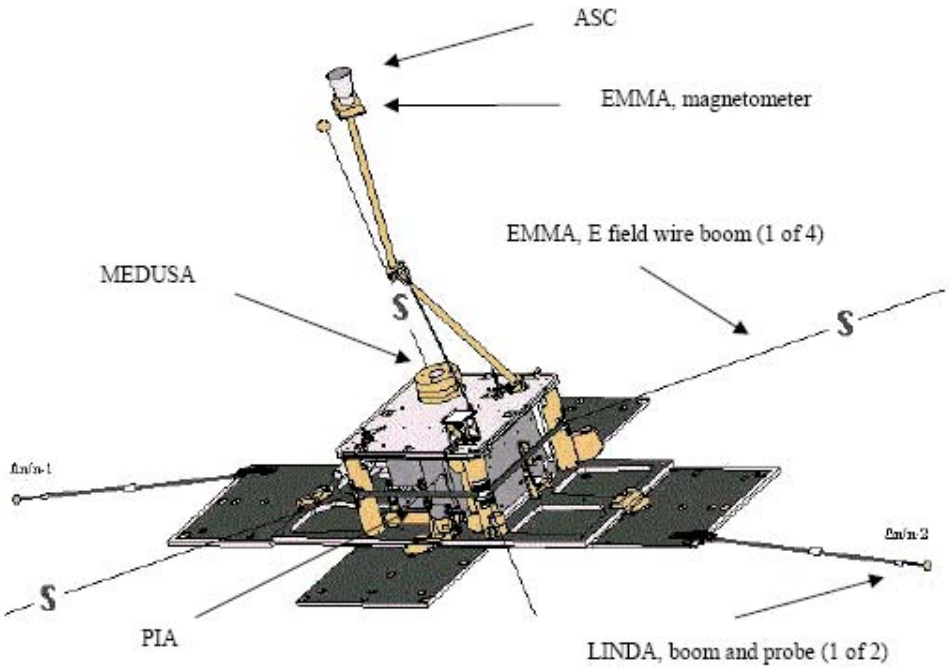

Figure 5.1: The Astrid-2 scientific playload. From Blomberg *et al.* [10].

The magnetic field was measured by a tri-axial fluxgate sensor located at the tip of a rigid boom extended along the spacecraft axis and facing away the Sun. A summary of some characteristics of the EMMA instrument are summarized in Table 5.1. A detailed description of the EMMA instrument is given by Blomberg *et al.* [10].

Quantity	Range	Resolution	Bits	Sample rate (s^{-1})
E(2 components)	± 5 V/m	0.03 mV/m	16	16, 256, 2048
B(3 components)	± 62 μT	0.12 nT	20	16, 256, 2048

Table 5.1: Summary of measured quantities.

5.2 The Cluster Spacecraft

The European Space Agency's (ESA) Cluster mission was designed to study the small-scale structures and the macroscopic turbulence in the magnetospheric and the near-Earth solar wind plasmas, in three dimensions [17]. It consists of four coordinated and identical spacecraft in a polar excentric orbit with a perigee of $\sim$4 R_E and an apogee of 19.6 R_E, with an orbital period of 57 hours. A perfect tetrahedron has been shown to be the best spacecraft configuration for the study of three dimensional structures [13]. The spacecraft therefore travel in a tetrahedron formation with variable size (from 200 to 18000 km) and configuration (from perfect tetrahedral to aligned). Different configuration and separation strategies are adopted depending on the target of each phase of the mission. Figure 5.2 shows a comparison of the Cluster orbit in 2009 (solid) and 2001 (dashed). The 2009 orbit passes through the subsolar magnetopause on the dayside and through the auroral acceleration region on the nightside.

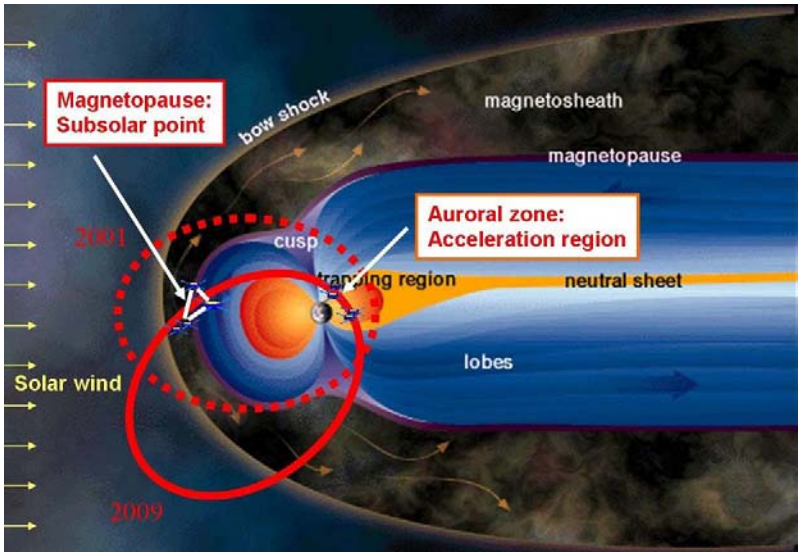

Figure 5.2: Cluster orbit on diagram of the Earth's magnetosphere. Image credit: ESA.

The Cluster spacecraft were launched in pairs by two Soyuz launchers on 16 July and 9 August 2000 from Baikonour, Kazahkstan. The spacecraft 1, 2, 3 and

4 were named Rumba, Salsa, Samba and Tango[1], respectively.

The four Cluster spacecraft are identical and each contains 11 instruments. In order to permit accurate inter-comparison between the measurements of each instrument on board the different spacecraft, special attention was given to a perfect manufacturing and a very precise calibration of each instrument. Table 5.2 shows a list of the different instruments and of the respective actual Principal Investigator.

Acronym	Instrument	Principal Investigator
FGM	FluxGate Magnetometer	E. Lucek (IC, UK)
STAFF	Spatial-Temporal Analysis of Field Fluctuation experiment	N. Cornilleau-Wehrlin (CETP, France)
EFW	Electric Field and Wave experiment	M. André (IRFU, Sweden)
WHISPER	Waves of HIgh frequency and Sounder for Probing of Electron density by Relaxation	J. G. Trotignon (LPCE, France)
WBD	Wide Band Data	J. Pickett (Iowa U., USA)
DWP	Digital Wave Processing experiment	H. Alleyne (Sheffield U., UK)
EDI	Electron Drift Instrument	R. B. Torbert (UNH, USA)
CIS	Cluster Ion Spectrometry	I. Dandouras (CESR, France)
PEACE	Plasma Electron And Current Experiment	A. Fazakerley (MSSL, UK)
RAPID	Research with Adaptive Particle Imaging Detectors	P. Daly (MPAe, Germany)
ASPOC	Active Spacecraft POtential Control	K. Torkar (IWF, Austria)

Table 5.2: Instruments on Cluster and actual Principal Investigators.

Measurements from the FGM, EFW, CIS and PEACE instruments are used in Papers 2 and 3 of this thesis. A concise description of the main characteristics of these four instruments is presented below.

FGM

The FGM instrument on board Cluster provides intercalibrated four-point measurements of the full magnetic field vector with high accuracy (about 0.1%) and high time-resolution (between 15.5 and 67.2 vectors s^{-1}). Each instrument consists of two triaxial fluxgate magnetometers and an on-board data-processing unit. In order to minimize the disturbances caused by the background fields due to the

[1]Watch the quartet of dancing satellites performing in the ESA's website http://sci.esa.int/science-e/www/object/index.cfm?fobjectid=22910&fareaid=8

spacecraft (which is the major potential source of uncertainties for magnetic-field measurements in space), the magnetometer sensors are mounted on radial booms at 4.7 and 6.2 m from the center-line of the spacecraft. The resulting background magnetic field at both sensors is 0.12 nT. A detailed description of the FGM instrument is given by Balogh *et al.* [5].

Measurements from the FGM instrument are used to estimate the field-aligned current density in Papers 2 and 3. The assumption of an infinite current sheet is used, which is often a fairly good approximation in the auroral region. The alignment of the current sheet is estimated using minimum/maximum variance analysis applied to the magnetic/electric field measurements, respectively. The direction which better minimizes the magnetic field variations and simultaneously better maximizes the electric field variations is considered to be the best approximation for the orientation of the current sheet. The field-aligned current density is then estimated from the gradient of the magnetic field component parallel to the current sheet along the perpendicular direction. This is a rather common method used for single-point measurements in space. The coordinated multi-point measurements from the Cluster spacecraft allow the use of a more advanced analysis tool called the curlometer technique. This method relies on the direct estimation of the current density from $\nabla \times \mathbf{B}$ using measured spatial gradients of the magnetic field and assuming that the four spacecraft are passing simultaneously through the same current sheet. This requires that the size of the tetrahedron formed by the Cluster spacecraft must be small enough so as to allow the gradients inside the tetrahedron to be as linear as possible, which is equivalent to say that the current remains constant inside the tetrahedron. The shape of the tetrahedral configuration is also important for the accuracy of the curlometer technique. Extreme distortions of the tetrahedron result of a poor accuracy on the determination of one or more of the components of the current. This technique is therefore not applicable for the cases investigated in Papers 2 and 3, when the Cluster spacecraft were nearly aligned as pearls on a string.

EFW

The EFW experiment [22] consists of four spherical probes numbered 1 to 4 located at the ends of 44 m long wire booms lying in the spin plane of the spacecraft. Direct measurements of the two spin plane components of the electric field are obtained from the potential difference between the two pairs of opposing probes (V12 and V34) divided by the distance between the probes (88 m), known as the double probe technique [18]. The electric field component along the spin axis can be reconstructed with the assumption $\mathbf{E} \cdot \mathbf{B} = 0$ when the magnetic field vector is known and makes a relatively large angle with the spin plane. The Cluster spacecraft pass the auroral region at geocentric altitudes of 4-7 R_E, typically well above the auroral acceleration regions, allowing the assumption $\mathbf{E} \cdot \mathbf{B} = 0$.

The probes can be operated in voltage mode to measure the electric field, or in current or Langmuir mode to measure the plasma density and the electron tem-

perature. In the voltage mode, a constant bias current is given to the probe. Its potential is then determined by the balance of the plasma electron current, the photoemission current, and the bias current to the probe. The magnitude of the applied bias current controls in this way the working point for the probe on the current-voltage characteristic curve. The preferable 'working point' is the one that gives the lowest probe-to-plasma impedance, and consequently the best measurements. In the current mode, the probe is given a bias voltage with reference to the satellite ground. By positively biasing the probe, an electron current proportional to the plasma density is collected, provided that the electron temperature is constant. Fluctuations in the plasma density are therefore reflected in fluctuations in the probe current.

In the low telemetry mode (normal mode) the measurements are limited to a time resolution of 25 samples/s, while in the high telemetry mode (burst mode) 450 samples/s can be obtained. The amplitude range of the quasi-static (DC) electric field measurements is 0.3-700 mV/m, while the oscillating (AC) electric field can be measured in the frequency range 50-8000 Hz and amplitude range 0.001-10 mV/m. The plasma density can be measured over a range of 1 to 100 cm^{-3} and the electron temperature in the eV range. Electric field data with a time resolution of 4 seconds (spin resolution) are also available and are the result of on-board least-square fit of a sine wave to one probe pair (P12 or P34) over 4 seconds.

The electric field measurements are made in the moving and spinning reference frame of the spacecraft. Therefore, the data must be transformed from the fixed satellite system into a geophysical coordinate system (this is normally called despinning), in order to be scientifically useful. The electric field induced by the motion of the satellite through the geomagnetic field must also be removed from the raw data.

There are several sources of spurious effects on the EFW measurements that one should be aware of when using the data [36]. A summary of the most important known effects are listed below. This summary closely follows the description presented by Yuri *et al.* [36].

Failure of Probe 1 on Cluster spacecraft 1, 2 and 3. A failure occurred on probe 1 on Cluster spacecraft 1 (28 December 2001), on spacecraft 3 (29 July 2002), and on spacecraft 2 (13 May 2007). The spin plane electric field is therefore no longer possible to calculate from the difference of the potential between opposing probes (P12 = P1 - P2 and P34 = P3 - P4) as it is done when all the probes are functional. However, a workaround was found to use P32 instead of P12, the so-called asymmetric mode. This was implemented on 29 September 2003 on spacecraft 1 and 3, and on 24 November 2007 on spacecraft 2. The computation of the electric field is equally straightforward in the asymmetric as in the symmetric mode, however the errors are larger in the former mode since the measured signals are not orthogonal. During the period that preceded the implementation of the asymmetric mode, full resolution measurements in the spinning system are available only from the

probe pair 34, and thus the electric field has a strong spin modulation. The spin resolution measurements of the electric field are however available and not affected by this failure.

Plasmasphere. Comparisons between the electric field measurements made by the EFW and the EDI instruments show that a spurious field of about 1-2 mV/m is sometimes measured mostly in the sunward component of the electric field measured by the EFW instrument, when the spacecraft is in the plasmapshere. The reasons of this disturbance are not yet fully understood.

Cold ion drift wakes. A large negatively charged wake may be formed behind the booms, when the spacecraft moves through regions of low density plasmas with a drifting cold ion population, such as in the tail lobes above the polar caps and in the low latitude dayside magnetosphere. As the individual probes enter and exit the wake there is a dip in the probe potential, that appears in the raw data signal as a spike twice per spin on each probe pair. The spurious electric field is substantially reduced when the ASPOC is operating, since the spacecraft potential is then kept at a much lower value, reducing therefore the effects of wakes due to cold ion drift.

Solar wind wakes. Spurious effects are also observed in the EFW electric field measurements when the spacecraft is moving through the near-Earth solar wind plasma. A negatively charged wake is formed behind the spacecraft in the direction of the solar wind flow.

Operations of other instruments The sounding waves emitted at certain frequencies by the WHISPER instrument are seen in the EFW measurements usually as spikes with a repetition period of 52 s or 104 s in the normal mode. The electron beams emitted by the EDI instrument also adversely affect the EFW data, contributing to the increase of the spacecraft potential, mainly in regions of low density plasma. The operation of the ASPOC instrument influences the EFW measurements in different ways. As mentioned before, cold plasma wake effects may be reduced when the ASPOC is operating. However, variable offsets are seen in the sunward component when ASPOC is operating, and the noise level may sometimes increase significantly at low frequencies.

Much efforts have been done to develop algorithms that identify and remove the above mentioned spurious effects from the EFW measurements. The validated data are available for the scientific community through the Cluster Active Archive[2] (CAA). However, the users should be aware that the detection of problematic intervals is not always perfect.

[2] http://caa.estec.esa.int/caa/home.xml

CIS and PEACE

The Cluster Ion Spectrometer (CIS) experiment [58] consists of two ion sensors able to measure the full three-dimensional ion distributions with a time resolution of one spacecraft spin period (4 s). The time-of-flight ion COmposition and DIstribution Function (CODIF) sensor measures the distributions of the major ions (H^+, He^+, He^{++}, and O^+) with energies from 1 eV to 40 keV with a 22.5° angular resolution. The Hot Ion Analyzer (HIA) sensor does not have mass resolution but has a better angular resolution capability (5.6° × 5.6°).

Another instrument monitoring the particle distributions within the plasma is the Plasma Electron And Current Experiment (PEACE) [29]. It consists of two sensors that measure the three-dimensional velocity distribution of the electrons in a dynamic energy range varying from 0.59 eV up to 26.4 keV, with a time resolution of half a spacecraft rotation. Partial distributions can be recorded with a time resolution of 62.5 ms while angular distributions at a fixed energy may be obtained with a period of 7.8 ms. The sensors are placed to view radially on opposite sides of the spacecraft and have an angular resolution of 2.8° and 5.3° respectively in the azimuthal direction, and 15° in the polar direction.

Chapter 6

Summary of Papers

6.1 Paper 1

Investigation of subauroral ion drifts and related field-aligned currents and ionospheric conductivity

This paper presents statistics on SAID occurrence based on a set of six months of data measured on board the Astrid-2 satellite. A subauroral ion drift event is defined as corresponding to a poleward electric field with magnitude greater than 30 mV/m at 1000 km altitude, with a latitudinal extension between 0.05° and 1.05°, and a location equatorward of the auroral oval. The results confirm that SAID events occur predominantly in the premidnight sector, with a maximum probability within the 20-23 MLT sector, where also the most rapid SAID events are found.

An anti-correlation is observed between the magnitude of the SAID electric field and its latitudinal width during substorm evolution, suggesting a voltage generator acting as the magnetospheric source for the SAID formation. However, estimates of the field-aligned current density and the height-integrated Pedersen conductivity distribution show that SAID events are associated with a reduction of the ionospheric conductivity, with the strongest electric field peaks corresponding to the lowest conductivity minimum values. This result indicates a magnetospheric current generator as the source for the SAID formation.

It is concluded that the SAID generation mechanism can neither be regarded as a pure voltage generator nor as a pure current magnetospheric generator, but as having certain characteristics of both types. Moreover, the clear modifications seen in the ionospheric Pedersen conductivity distribution associated with the SAID structure as time evolves, indicate that the ionospheric response is of importance for sustaining and modifying the SAID structures.

6.2 Paper 2

Temporal and spatial evolution of discrete auroral arcs as seen by Cluster

The temporal and spatial evolution of two events observed by the Cluster spacecraft at the inner and outer edges of the plasma sheet boundary layer, in the 20-21 MLT sector, is investigated in this paper. Both events are characterized by electric field variations of up to ∼1350 mV/m mapped magnitude associated with negative potential structures and upward ion beams, and occur in the upward current region.

Event 1 occurs under rather quiet auroral conditions during the end of a substorm, in the vicinity of the boundary between the plasma sheet and the plasma sheet boundary layer, at about 4 R_E altitude. A system of auroral arcs with a perpendicular potential drop of about 10 kV is observed showing a rather dynamic evolution in time. The auroral arc structures merge, broaden and intensify during a time interval of about 50 minutes, after which the arcs fade away. The PS region as well as the arc structure located at its poleward edge remain relatively fixed in space. For this particular event, a part of the auroral upward acceleration region extends beyond 3.9 R_E altitude, as indicated by the observation of inverted-V electrons moving in the downward field-aligned direction.

Event 2 occurs during the expansion phase of a substorm with the Cluster spacecraft passing above the horn region of a surge-type aurora. Conjugate observations by the South Pole All Sky Imager and by the DMSP F13 spacecraft show an east-west aligned auroral arc, 30 to 50 km wide. This auroral arc maps to the outer edge of the plasma sheet boundary layer, where strong electric field variations and field-aligned currents are measured by the Cluster spacecraft at an altitude of about 4.6 R_E. The observations show that this auroral arc consists of multiple small-scale arcs which later merge into one structure and intensify at the PSBL outer edge. The multi-point observations by the four Cluster spacecraft show the poleward motion of the surge horn and the associated PSBL with a velocity of 0.5 km/s (mapped to the ionosphere), in accordance with the poleward expansion of the auroral oval during the substorm expansion phase.

6.3 Paper 3

Magnetosphere-ionosphere coupling during periods of extended high auroral activity: a case study

A case study is presented using Cluster data from a crossing of the boundary between the southern magnetotail lobe and the PSBL during a period of extended high auroral activity, so called HILDCAA period. The data show a multi-layered boundary with temporal or spatial variations in the different layers. Upward accelerated H^+ and O^+ ion beams are detected associated with both quasi-static potential structures and with large-amplitude and low-frequency electric field fluc-

tuations, suggesting that the parallel acceleration occurs by means of field-aligned electric fields and by magnetic pumping, respectively. The comparison of the energy of the ion beams with the perpendicular potential estimated from the integral along the orbit of the measured electric field shows a mismatch, indicating that temporal changes of the acceleration region might occur during the time that it takes for the ions to travel from the acceleration region up to Cluster altitudes.

Intense field-aligned Poynting fluxes directed upward away from the ionosphere are measured associated with the regions of quasi-static electric field structures, suggesting that these structures are magnetically coupled to and partly generated in the lower ionosphere. The generation of the ionospheric electric fields, that are magnetically linked to higher altitudes, may possibly occur due the requirement of current closure across an ionospheric density gradient associated with the ionospheric projection of the PSBL outer edge. The propagation toward higher altitudes of the resultant changes in the potential distribution is reflected in the observed upward propagating field-aligned Poynting fluxes. Moreover, it seems probable that the coupling between the low ionosphere and the magnetosphere is favored during periods of extended auroral activity, since the ionosphere has in this case sufficiently long time to respond to the enhanced energy inputs.

6.4 Paper 4

Statistical study on the occurrence of ASAID electric fields

Electric and magnetic field data from the Astrid-2 satellite are used in this study to investigate the occurrence of ASAID. The selection of the ASAID events is based on two criteria: the electric fields are directed mainly equatorward and are located in the vicinity of the equatorward edge of the auroral oval or equatorward of it.

The selected events show electric field magnitudes between 45 mV/m and 185 mV/m and latitudinal extensions between 0.2° and 1.2°, in a few cases up to 3.0°. They occur predominantly in the 23 to 3 MLT sector, and all the events are located very near to the equatorward edge of the auroral oval. A major difference between ASAID and SAID is their relation to substorm activity. While SAID is well know to be substorm-related, often occurring during the recovery phase of substorms, ASAID are seen to occur mainly during extended periods of low substorm activity.

ASAID events are associated with a FAC system with similar scale size as the ASAID channel, composed of a downward FAC flowing at the poleward edge of the ASAID structure and an upward FAC flowing at its equatorward edge. The current density varies between 0.5 and 2.0 $\mu A/m^2$. The good correlation seen between the variations of the electric and the magnetic fields suggest that the ionospheric conductivity is rather homogeneous in the ASAID region, meaning that the ASAID structures do not contribute significantly to the reduction of the ionospheric conductivity.

A discussion of different mechanisms that possibly may generate ASAID electric fields is presented. However, the fact that the observations used in this study are

restricted to the ionospheric end of the ASAID flux tubes, limits our discussion to more hypothetical scenarios. The proximity of the electron and the ion plasma sheet inner boundaries, as well as of the ring current outer edge and the plasmapause, during extended quiet times, are believed to be of major importance for the generation of ASAID electric fields.

Chapter 7

Discussion and Conclusions

This thesis is about the electrodynamics of two distinct magnetosphere-ionosphere coupling phenomena. These are auroral electric fields in the upward current region and subauroral electric fields. Both have in common the fact that they occur at plasma boundaries regions magnetically linked to the nightside auroral ionosphere, and that they result from a dynamic coupling between the ionosphere and the magnetosphere. However, whereas the subauroral electric fields are relatively large-scale and couple between the magnetosphere and the ionosphere, the auroral electric fields are typically smaller-scale and mainly decoupled.

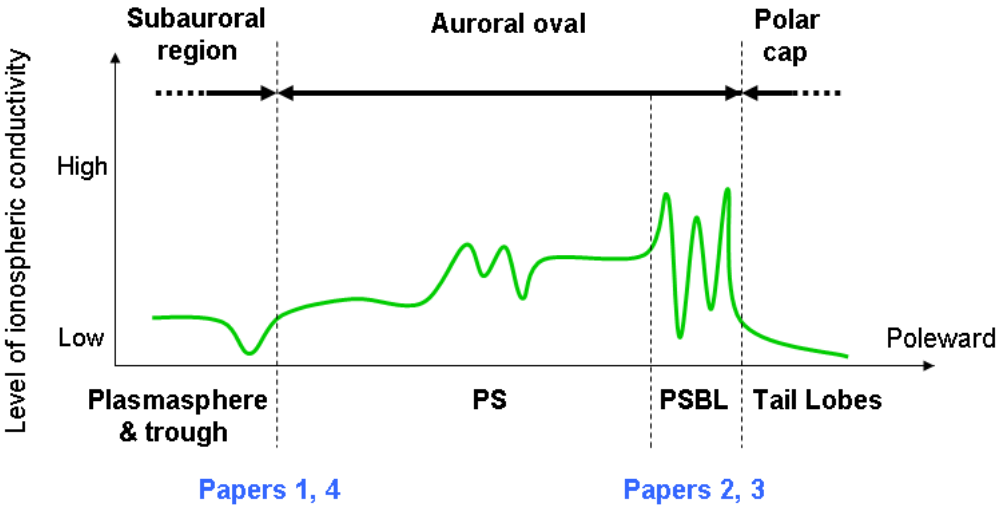

Figure 7.1: Schematic representation of the level of height-integrated Pedersen conductivity in the nightside ionosphere as a function of the latitude.

Figure 7.1 is a schematic representation of the level of height-integrated Pedersen conductivity in the nightside ionosphere as a function of the latitude. The three distinct plasma boundaries discussed in this thesis are marked with vertical dashed lines. These are the plasma sheet inner boundary, and the inner and the outer edges of the plasma sheet boundary layer. The papers that discuss each of these boundaries are indicated at the bottom of the figure.

Paper 1 and Paper 4 deal with subauroral electric fields observed in the vicinity or Earthward of the plasma sheet inner boundary, whereas Paper 2 and Paper 3 discuss the electrodynamics of auroral structures observed at the inner and the outer edges of the plasma sheet boundary layer. The dip in the level of ionospheric conductivity in the region equatorward of the auroral oval's equatorward edge, refers to the midlatitude trough, that is typically observed in the nightside subauroral ionosphere. The level of ionospheric conductivity is typically higher in the auroral region than in the subauroral region, showing variations that can be rather significant close to the poleward edge of the auroral oval, to where the plasma sheet boundary layer is magnetically linked.

High altitude multi-point measurements from the Cluster spacecraft are used in Paper 2 to analyze the spatial and temporal characteristics of auroral structures in the upward current region. The upward extension of the equipotentials of U- and S-shaped potential structures are seen to extend up to altitudes between 4 R_E and 4.6 R_E, confirming previous similar results [75]. Conjugate observations between the Cluster spacecraft, the DMSP F13 spacecraft and the South Pole All Sky Imager available for some of these structures, show that they correspond to auroral arc structures with scale-sizes of 15-50 km (mapped to the ionosphere), associated with potential drops between 9 and 15 kV, located at the inner edge of the plasma sheet boundary layer. Furthermore, the observation of an inverted-V-like distribution for downgoing electrons for one of the events, indicates that the spacecraft is crossing through the auroral acceleration region. The peak energy of this inverted-V distribution was $\sim$800 eV and it is measured at 3.9 R_E altitude. The auroral upward acceleration region, that is typically located between 2000 km and 2 R_E altitude [57] (Section 3.2), is for this case seen to extend beyond 3.9 R_E altitudes.

The observed auroral structures change dynamically in shape and magnitude, merging, broadening, intensifying and fading away during a time interval of $\sim$50 minutes. They appear however to be fixed to the inner edge of the plasma sheet boundary layer, where they are originally formed. The ionospheric response generated at this boundary is strongly affected by the associated ionospheric conductivity gradient, and by the high-altitude dilute plasma conditions, being crucial for the maintenance of the observed magnetospheric potential structures.

The importance of the ionosphere for the formation, maintenance and dynamics of potential structures in the downward current region have been demonstrated in several studies [71, 72, 73]. They have shown that the generation of small-scale and intense low-altitude magnetospheric electric fields requires a reduction of the ionospheric conductivity in the corresponding mapped region. This is most likely

to occur in the downward current region where the electrons are evacuated from the ionosphere by the FACs, explaining why the strongest small-scale (4-5 km mapped to the ionosphere) electric fields are most commonly observed in the downward current region.

The results presented in Paper 2 of this thesis show that the magnetosphere-ionosphere coupling along magnetic field lines threading plasma boundary regions, create conditions that are favorable for the formation and maintenance of intense magnetospheric electric fields, also in the upward current region. The understanding of the effects of upward field aligned currents flowing at such boundary regions, and of the associated ionospheric response generated at the mapped ionospheric density gradient, needs further investigation.

Electric field, magnetic field and particle data measured on board the Cluster spacecraft 1, when crossing through the outer boundary region of the PSBL, is used in Paper 3 to demonstrate the complexity of this boundary region, and the magnetosphere-ionosphere coupling in the upward current region, during a period of extended high auroral activity.

The results show that the boundary region is composed of several small-scale layers, where quasi-static potential structures and low-frequency electric field variations are observed in the different layers, accelerating the ions in the upward field-aligned direction. The strongest quasi-static electric field structures have peak amplitudes of about 1.2 V/m and 1.5 V/m, and have rather small scale-sizes, $\sim$2 km and 7 km (these values are mapped to 100 km altitude). Furthermore, they are associated with intense field-aligned Poynting fluxes directed upward away from the ionosphere with mapped magnitudes between 400 mW/m^2 and 600 mW/m^2.

These observations suggest that the ionospheric response contributes in this case significantly to the formation of the strong and small-scale convergent electric fields observed by the Cluster spacecraft in the upward current region, similar to what has been found in simulations by Streltsov and Marklund [73] for the downward current region. This result illustrates the complexity of the coupling processes in plasma boundary regions. Moreover, it shows that the magnetosphere-ionosphere coupling may be intensified during extended periods of efficient energy transfer along the solar wind-magnetosphere-ionosphere transmission chain, which seems probable since the ionosphere has in this case longer time to store excess dissipation energy and to respond to the enhanced energy inputs.

The other part of this thesis is about the formation of strong electric fields in narrow latitudinal channels, located in the vicinity or Earthward of the plasma sheet inner edge. These electric fields are associated with rapid ionospheric drift flows at the equatorward boundary of the auroral oval or equatorward of it, and are therefore called subauroral ion drifts. This topic is further discussed in Chapter 4, and is the subject of investigation in Paper 1 and in Paper 4.

The results presented in these papers show that strong subauroral electric fields are poleward- or equatorward-directed, have magnitudes most commonly between 30 mV/m and 150 mV/m, but even up to 400 mV/m, and are often confined to latitudinal extensions of about 0.1° to 1.2° (these values refer to an altitude of

1000 km). The results also indicate that the generator mechanism of the poleward-directed subauroral electric fields (SAID) has certain signatures of both a voltage and a current generator, and can not simply be described by one of these. The low conductivity of the subauroral ionosphere, accentuated in the premidnight sector where the midlatitude trough is deeper, together with the flow of downward FACs in the SAID region, appear to be important keys for the generation of the SAID electric fields.

The occurrence of equatorward-directed subauroral electric fields (ASAID) is investigated in Paper 4. Although this phenomenon is similar to SAID in some aspects, such as the electric field magnitude, the typical scale-size, the density of the associated FACs, and the location in the vicinity of the equatorward edge of the auroral oval, it differs clearly in other aspects such as the MLT location, the relation to substorm activity, and the association with modifications of the ionospheric conductivity. The close locations of the inner boundaries of the ion and the electron plasma sheets, and of the plasmapause and the outer edge of the ring current, are likely to be key factors for the generation of ASAID electric fields, justifying their occurrence during extended periods of low substorm activity.

Chapter 8

Future Work

While the SAID phenomenon has been the subject of many studies during the last three decades, the first observations of ASAID were reported less than one year ago, and were based on measurements from low-altitude orbiting satellites and from ground-based instruments. Extremely interesting would be the study of ASAID based on multipoint measurements made in the vicinity of the plasmapause. Unfortunately the measurements made by the Cluster EFW instrument are often strongly negatively affected by a spurious field measured when the spacecraft crosses the plasmasphere. However, the EDI instrument is expected to supply very interesting data from this region.

Multipoint measurements are enormously valuable for the further understanding of the coupling between the magnetosphere and the auroral and the subauroral ionospheres. Cluster measurements made during the year 2009 will certainly lead to very fruitful advances in the field of auroral physics, since the configuration of the spacecraft will allow conjugate measurements at different altitudes in the acceleration regions of the auroral zone. A similar configuration of multi-spacecraft at magnetically conjugate locations orbiting at midlatitudes, together with ground-based measurements of plasma flow, would benefit the further understanding of subauroral phenomena such as SAID and ASAID.

Numerical modeling is a useful tool for the interpretation of data. Several numerical studies have been published on the modeling of the magnetosphere-ionosphere coupling in the downward current region. Simulations of the upward flow of field-aligned currents in plasma boundary regions, considering the associated ionospheric density gradient, have however not yet been done. The consideration of the level and duration of auroral activity would also be interesting, since it is likely to affect the ionospheric response time.

Modeling of the dynamics of the inner magnetosphere during extended quiet periods would be interesting for the investigation of possible causes for the generation of ASAID electric fields.

Bibliography

[1] H. Alfvén. On the theory of magnetic storms and aurora. *Tellus*, 10:104, 1958.

[2] H. Alfvén. Existence of electromagnetic-hydrodynamic waves. *Nature*, 150:405, 1942.

[3] P. C. Anderson, W. B. Hanson, R. A. Heelis, J. D. Craven, N. D. Baker, and L. A. Frank. A proposed production model of rapid subauroal ion drifts and their relation to substorm evolution. *J. Geophys. Res.*, 98:6069–6078, 1993.

[4] P. C. Anderson, R. A. Heelis, and W. B. Hanson. The ionospheric signatures of rapid subauroral ion drifts. *J. Geophys. Res.*, 96:5785–5792, 1991.

[5] A. Balogh, M. W. Dunlop, S. W. Cowley, D. J. Southwood, J. G. Thomlinson, K. H. Glassmeier, G. Musmann, H. Lühr, S. Buchert, M. H. Acuña, D. H. Fairfield, J. A. Slavin, W. Riedler, K. Schwingenschuh, and M. G. Kivelson. Satellite measurements and theories of low altitude auroral particle acceleration. *Space Sci. Rev.*, 79:33–64, 1997.

[6] P. M. Banks. The thermal structure of the ionosphere. *Proceedings of the IEEE*, 57(3):258–281, 1969.

[7] W. Baumjohann and R. A. Treumann. *Basic Space Plasma Physics*. Imperial College Press, 1997.

[8] M. Blanc, J. L. Horwitz, J. Blake, I. A. Daglis, J. Lemaire, M. B. Moldwin, S. Orsini, R. Thorne, and R. A. Wolf. Source and loss processes in the inner magnetosphere. *In: B. Hultqvist, M. Oieroset, G. Paschmann, and R. Treumann (eds.): Magnetospheric Plasma Source and Losses*, 6 of Space Science Series of ISSI:137, 1999.

[9] L. P. Block and C. G. Fälthammar. The role of magnetic-field-aligned electric fields in auroral acceleration. *J. Geophys. Res.*, 95:5877, 1990.

[10] L. G. Blomberg, G. T. Marklund, P. A. Lindqvist, F. Primdahl, P. Brauer, L. Bylander, J. A. Cumnock, S. Eriksson, N. Ivchenko, T. Karlsson, A. Kullen, J. M. G. Merayo, E. B. Pedersen, and J. R. Petersen. EMMA - the Electric and

Magnetic Monitor of the Aurora on Astrid-2. *Ann. Geophysicae*, 22:115–123, 2004.

[11] P. Carlqvist and R. Boström. Space-charge regions above the aurora. *J. Geophys. Res.*, 75:7140–7146, 1970.

[12] C. C. Chaston, L. M. Peticolas, J. W. Bonnell, C. W. Carlson, R. E. Ergun, J. P. McFadden, and R. J. Strangeway. Width and brightness of auroral arcs driven by inertial alfven waves. *J. Geophys. Res.*, 108(A2):SIA 17–1, 2003.

[13] O. Coeur-Joly, P. Robert, G. Chanteur, and A. Roux. Simulated daily summaries of cluster four-point magnetic field measurements. *Proceedings of the Cluster Workshop on Physical Measurements and Mission-Oriented Theory*, ESA:223, 1995.

[14] J. De Keyser. Formation and evolution of subauroral ion drifts in the course of a substorm. *J. Geophys. Res.*, 104:12339–12349, 1999.

[15] T. E. Eastman, L. A. Frank, W. K. Peterson, and W. Lennartsson. The plasma sheet boundary layer. *J. Geophys. Res.*, 89:1553–1572, 1984.

[16] Y. Ebihara, N. Nishitani, T. Kikuchi, T. Ogawa, K. Hosokawa, and M.-C. Fok. Two-dimensional observations of overshielding during a magnetic storm by the Super Dual Auroral Radar Network (SuperDARN) Hokkaido radar. *J. Geophys. Res.*, 113:A01213, doi:10.1029/2007JA012641, 2008.

[17] C. P. Escoubet and R. Schmidt. Cluster II: Plasma measurements in three dimensions. *Adv. Space Rec.*, 25(8):1305–1314, 2000.

[18] U. Fahleson. Theory of electric field measurements conducted in the magnetosphere with electric probes. *Space Sci. Rev.*, 7:238–262, 1967.

[19] J. C. Foster and H. B. Vo. Average characteristics and activity dependence of the subauroral polarization stream. *J. Geophys. Res.*, 107:A12, doi:10.1029/2002JA009409, 2002.

[20] Y. I. Galperin, V. N. Ponomarev, and A. G. Zosimova. Plasma convection in the polar ionosphere. *Ann. Geophysicae*, 30:1–7, 1974.

[21] Y. I. Galperin, V. S. Soloviev, K. Torkar, J. C. Foster, and M. V. Veselov. Predicting plasmaspheric radial density profiles. *J. Geophys. Res.*, 102:2079–2091, 1997.

[22] G. Gustafsson, R. Boström, B. Holback, G. Holmgren, A. Lundgren, K. Stasiewicz, L. Åhlén, F. S. Mozer, D. Pankow, P. Harvey, P. Berg, R. Ulrich, A. Pedersen, R. Schmidt, A. Butler, A. W. C. Fransen, D. Klinge, C. G. Fälthammar, P. A. Lindqvist, S. Christenson, J. Holtet, B. Lybekk, T. A. Sten, P. Tanskanen, K. Lappalainen, and J. Wygant. The Electric Field and Wave experiment for the Cluster mission. *Space Sci. Rev.*, 79:137–156, 1997.

[23] W. B. Hanson. *Structure of the ionosphere, in Satellite Environment Handbook, Ed. F. S. Johnson.* Stanford University Press, 1965.

[24] R. A. Heelis, R. A. Spiro, W. B. Hanson, and J. L. Burch. Magnetosphere ionosphere coupling in the mid-latitude trough. *Trans. Am. Geophys. Union*, 57:990–991, 1976.

[25] A. J. Hundhausen. *The solar wind.* Introduction to Space Physics, Edited by Margaret G. Kivelson and Christopher T. Russell, pp. 586. ISBN 0521451043. Cambridge, UK: Cambridge University Press, April 1995., Apr. 1995.

[26] K. J. Hwang, K. A. Lynch, C. W. Carlson, J. W. Bonnell, and W. J. Peria. Fast Auroral Snapshot observations of perpendicular DC electric field structures in downward current regions: Implications. *J. Geophys. Res.*, 111(A09206):doi:10.1029/2005JA011472, 2006.

[27] T. Iijima and T. A. Potemra. Large-scale characteristics of field-aligned currents associated with substorms. *J. Geophys. Res.*, 83:599–615, 1978.

[28] T. Johansson, S. Figueiredo, T. Karlsson, G. Marklund, A. Fazakerley, S. Buchert, and H. Lindqvist, P. A.and Nilsson. Intense high-altitude auroral electric fields - temporal and spatial characteristics. *Ann. Geophysicae*, 22:2485–2495, 2004.

[29] A. D. Johnstone, C. Alsop, S. Burge, P. J. Carter, A. J. Coates, A. J. Coker, A. N. Fazakerley, M. Grande, R. A. Gowen, C. Gurgiolo, B. K. Hancock, B. Narheim, A. Preece, P. H. Sheathier, J. D. Winningham, and R. D. Woodliffe. PEACE: A Plasma Electron And Current Experiment. *Space Sci. Rev.*, 79:351–398, 1997.

[30] A. M. Jorgensen, H. E. Spence, W. J. Hughes, and H. J. Singer. A statistical study of the global structure of the ring current. *J. Geophys. Res.*, 109:A12204, doi:10.1029/2003JA010090, 2004.

[31] T. Karlsson, G. T. Marklund, L. G. Blomberg, and A. Mälkki. Subauroral electric fields observed by the Freja satellite: A statistical study. *J. Geophys. Res.*, 103:4327–4341, 1998.

[32] A. Keiling, J. R. Wygant, C. Cattell, W. Peria, G. Parks, M. Temerin, F. S. Mozer, C. T. Russell, and C. A. Kletzing. Correlation of Alfvén wave Poynting flux in the plasma sheet at 4-7 R_E with ionospheric electron energy flux. *J. Geophys. Res.*, 107(A7):1132, doi:10.1029/2001JA900140, 2002.

[33] A. Keiling, J. R. Wygant, C. A. Cattell, F. S. Mozer, and C. T. Russell. The global morphology of wave poynting flux: powering the aurora. *Science*, 299:383–386, 2003.

[34] M. C. Kelley, B. G. Fejer, and C. A. Gonzales. An explanation for anomalous ionospheric electric fields associated with a northward turning of the interplanetary magnetic field. *Geophys. Res. Lett.*, 6:301–304, 1979.

[35] J. D. Keyser, M. Roth, and J. Lemaire. The magnetospheric driver of subauroral ion drifts. *Geophys. Res. Lett.*, 25:1625–1628, 1998.

[36] Y. Khotyaintsev, P.-A. Lindqvist, A. Eriksson, and M. André. *The Cluster Book*. 2009.

[37] J. Kimball and T. J. Hallinan. Observations of black auroral patches and of their relationship to other types of aurora. *J. Geophys. Res.*, 103:14671–14682, 1998.

[38] M. G. Kivelson and C. T. Russell. *Introduction to Space Physics*. Introduction to Space Physics, Edited by Margaret G. Kivelson and Christopher T. Russell, pp. 586. ISBN 0521451043. Cambridge, UK: Cambridge University Press, April 1995., Apr. 1995.

[39] S. Knight. Parallel electric fields. *Planet. Space Sci.*, 21:741–750, 1973.

[40] L. R. Lyons, D. S. Evans, and R. Lundin. An observed relation between magnetic field aligned electric fields and downward electron energy fluxes in the vicinity of auroral forms. *J. Geophys. Res.*, 84, 1979.

[41] R. L. Lysak and Y. Song. Energetics of the ionospheric feedback instability. *J. Geophys. Res.*, 107(A8):doi:10.1029/2001JA000308, 2002.

[42] G. Marklund, L. Blomberg, C.-G. Falthammar, and P.-A. Lindqvist. On intense diverging electric fields associated with black aurora. *Geophys. Res. Lett.*, 21:1859–1862, 1994.

[43] G. Marklund, T. Karlsson, and J. Clemmons. On low-altitude particle acceleration and intense electric fields and their relationship to black aurora. *J. Geophys. Res.*, 102:17509–17522, 1997.

[44] G. T. Marklund, N. Ivchenko, T. Karlsson, A. Fazakerley, M. Dunlop, P. A. Lindqvist, S. Buchert, C. Owen, M. Taylor, A. Vaivalds, P. Carter, M. Andr*é*, and A. Balogh. Temporal evolution of the electric field accelerating electrons away from the auroral ionosphere. *Nature*, 414:724–727, 2001.

[45] M. C. Maynard. On large poleward-directed electric fields at sub-auroral latitudes. *Geophys. Res. Lett.*, 5:617–618, 1978.

[46] N. C. Maynard, T. L. Aggson, and J. P. Heppner. Magnetospheric observations of large sub-auroral electric fields. *Geophys. Res. Lett.*, 7:881–884, 1980.

[47] J. P. McFadden, C. W. Carlson, and R. E. Ergun. Microstructure of the auroral acceleration region as observed by FAST. *J. Geophys. Res.*, 104:14453–14480, 1999.

[48] C. E. McIlwain. Direct measurement of particles producing visible auroras. *J. Geophys. Res.*, 65:2727, 1960.

[49] R. J. Moffett, B. Jenkins, and G. J. Bailey. A modelling study of anisotropic ion temperatures generated in the F-layer by subauroral ion drifts. *Ann. Geophysicae*, 11:1051–1063, 1993.

[50] F. S. Mozer. On the lowest altitude $S3-3$ obervations of electrostatic shocks and parallel electric fields. *Geophys. Res. Lett.*, 7:1097–1098, 1980.

[51] F. S. Mozer and A. Hull. Origin and geometry of upward parallel electric fields in the auroral acceleration region. *J. Geophys. Res.*, 106:5763–5778, 2001.

[52] Y. Nishimura, J. Wygant, T. Ono, M. Iizima, A. Kumamoto, D. Brautigam, and R. Friedel. Saps measurements around the magnetic equator by crres. *Geophys. Res. Lett.*, 35:L10104, doi:10.1029/2008GL033970, 2008.

[53] D. M. Ober and J. L. Horwitz. Formation of density troughs embedded in the outer plasmasphere by subauroral ion drift events. *J. Geophys. Res.*, 102:14595–14602, 1997.

[54] G. Paschmann, S. Haaland, and R. Treumann. *Auroral Plasma Physics*. Springer, 2003.

[55] J. F. Providakes, M. C. Kelley, and W. E. Swartz. Radar and optical measurements of ionospheric processes associated with intense subauroral electric fields. *J. Geophys. Res.*, 94:5350–5366, 1989.

[56] P. A. Puhl-Quinn, H. Matsui, E. Mishin, C. Mouikis, L. Kistler, Y. Khotyaintsev, P. M. E. Décréau, and E. Lucek. Cluster and dmsp observations of said electric fields. *J. Geophys. Res.*, 112:A05219, doi:10.1029/2006JA012065, 2007.

[57] P. H. Reiff, G. Lu, J. L. Burch, J. D. Winningham, L. A. Frank, J. D. Craven, W. K. Peterson, and R. A. Heelis. On the high- and low-altitude limits of the auroral electric field region. *Auroral Plasma Dynamics, Geophysical Monograph 80, AGU*, pages 143–154, 1993.

[58] H. Rème, J. M. Bosqued, J. A. Sauvaud, A. Cros, J. Dandouras, C. Aoustin, J. Bouyssou, T. Camus, J. Cuvilo, C. Martz, J. L. Médale, H. Perrier, D. Romefort, J. Rouzaud, C. d'Uston, E. Möbius, K. Crocker, M. Granoff, L. M. Kistler, M. Popecki, D. Hovestadt, B. Klecker, G. Paschmann, M. Scholer, C. W. Carlson, D. W. Curtis, R. P. Lin, J. P. McFadden, V. Formisano, E. Amata, M. B. Bavassano-Cattaneo, P. Baldetti, G. Belluci, R. Bruno, G. Chionchio, A. d.

Lellis, E. G. Shelley, A. G. Ghielmetti, W. Lennartsson, A. Korth, H. Rosenbauer, R. Lundin, S. Olsen, G. K. Parks, M. McCarthy, and H. Balsiger. The Cluster Ion Spectrometry [CIS] Experiment. *Space Sci. Rev.*, 79:303–350, 1997.

[59] F. J. Rich, W. J. Burke, M. C. Kelley, and M. Smiddy. Observations of field-aligned currents in association with strong convection electric fields at subauroral latitudes. *J. Geophys. Res.*, 85:2335–2340, 1980.

[60] A. S. Rodger, R. J. Moffett, and S. Quegan. The role of ion drift in the formation of ionisation troughs in the mid- and high-latitude ionosphere - a review. *J. atmos. terr. Phys.*, 54:1–30, 1992.

[61] T. M. Schumaker, D. H. Gussenhoven, and R. Carovillano. The relationship between diffuse auroral and plasma sheet electron distributions near local midnight. *J. Geophys. Res.*, 94:10061, 1989.

[62] R. W. Schunk and P. M. Banks. Effects of electric fields and other processes upon the nighttime high-latitude *F* layer. *J. Geophys. Res.*, 81:3271–3282, 1976.

[63] E. G. Shelley, R. D. Sharp, and R. G. Johnson. Satellite observations of an ionospheric acceleration mechanism. *Geophys. Res. Lett.*, 3:654–656, 1976.

[64] M. Smiddy, M. C. Kelley, W. Burke, F. Rich, R. Sagalyn, B. Schuman, R. Hays, and S. Lai. Intense poleward-directed electric fields near the ionospheric projection of the plasmapause. *Geophys. Res. Lett.*, 4:543–546, 1977.

[65] D. J. Southwood. An assessment of the role of precipitation in magnetospheric convection. *J. Geophys. Res.*, 83, A11:5227–5232, 1978.

[66] R. W. Spiro, W. B. Hanson, D. L. Sterling, and R. A. Hoffman. Midlatitude trough characteristics as observed by atmosphere explorer. *Trans. Am. Geophys. Union*, 55:1159, 1974.

[67] R. W. Spiro, R. H. Heelis, and W. B. Hanson. Rapid sub-auroral ion drifts observed by Atmospheric Explorer C. *Geophys. Res. Lett.*, 6:657–660, 1979.

[68] R. W. Spiro and R. A. Wolf. Electrodynamics of convection in the inner magnetosphere. *Magnetospheric Currents, Geophys. Monogr. Ser.*, 28:248, 2007.

[69] R. W. Spiro, R. A. Wolf, and B. G. Fejer. Penetration of high-latitude-electric-field effects to low latitudes during SUNDIAL 1984. *Ann. Geophysicae*, 6:39–49, 1988.

[70] D. P. Stern. The art of mapping the magnetosphere. *J. Geophys. Res.*, 99, 1994.

[71] A. V. Streltsov and W. Lotko. Small-scale electric fields in downward auroral current channels. *J. Geophys. Res.*, 108(A7):doi:10.1029/2002JA009806, 2003.

[72] A. V. Streltsov and W. Lotko. Multiscale electrodynamics of the ionosphere-magnetosphere system. *J. Geophys. Res.*, 109:A09214, doi:10.1029/2004JA010457, 2004.

[73] A. V. Streltsov and G. T. Marklund. Divergent electric fields in downward current channels. *J. Geophys. Res.*, 111:A07204, doi:10.1029/2005JA011196, 2006.

[74] T. S. Trondsen and L. L. Cogger. High-resolution television observations of black aurora. *J. Geophys. Res.*, 102:363–378, 1997.

[75] A. Vaivads, M. André, S. Buchert, A. I. Eriksson, A. Olsson, J. E. Wahlund, P. Janhunen, G. Marklund, L. M. Kistler, C. Mouikis, D. Winningham, A. Fazakerley, and P. Newell. What high altitude observations tell us about the auroral acceleration: a Cluster/DMSP conjunction. *Geophys. Res. Lett.*, 30:1106, doi:10.1029/2002GL016006, 2003.

[76] V. M. Vasyliunas. Low-energy electrons in the magnetosphere as observed by OGO-1 and OGO-3. *Physics of the Magnetosphere, ed R. L. Carovillano, Dordrect: Reidel*, page 622, 1968.

[77] V. M. Vasyliunas. The interrelationship of magnetospheric processes. *The Earth's magnetospheric processes*, pages 29–38, 1972.

[78] J. Vedin and K. Rönnmark. Electrostatic potentials in the downward auroral current region. *J. Geophys. Res.*, 110:A08207,doi:10.1029/2005JA011083, 2005.

[79] M. Voiculescu and M. Roth. Eastward sub-auroral ion drifts or ASAID. *Ann. Geophysicae*, 26:1955–1963, www.ann–geophys.net/26/1955/2008/, 2008.

[80] Wikipedia. L-shell [online] available at: http://en.wikipedia.org/wiki/l-shell. page [accessed on 31 Mars 2009], 2008.

[81] R. A. Wolf. Effects of ionospheric conductivity on convection flow of plasma in the magnetosphere. *J. Geophys. Res.*, 75:4677–4698, 1970.

[82] R. A. Wolf. Calculations of magnetospheric electric fields. *Magnetospheric physics*, pages 167–177, 1974.

[83] R. A. Wolf. *Magnetospheric configuration.* Introduction to Space Physics, Edited by Margaret G. Kivelson and Christopher T. Russell, pp. 586. ISBN 0521451043. Cambridge, UK: Cambridge University Press, April 1995., Apr. 1995.

[84] J. R. Wygant, A. Keiling, C. A. Cattell, R. L. Lysak, M. Temerin, F. S. Mozer, C. A. Kletzing, J. D. Scudder, V. Streltsov, W. Lotko, and C. T. Russell. Some properties of Alvén waves: Observations in the tail lobes and the plasma sheet

boundary layer. *J. Geophys. Res.*, 107(A8):1201, doi:10.1029/2001JA900113, 2002.

[85] H. C. Yeh, J. C. Foster, F. J. Rich, and W. Swider. Storm time electric field penetration observed at mid-latitude. *J. Geophys. Res.*, 96:5707–5721, 1991.